uc3m | Universidad Carlos III de Madrid

Degree in Biomedical Engineering

2017-2018

Final Degree Project

"Generation of a Blister Model by Disruption of the Dermal-Epidermal Junction for Diagnosis of Recessive Dystrophic Epidermolysis Bullosa"

Lucía Marinas del Rey

Tutors

Marta García Díez

Francisco Javier Quero Lombardero

Leganés, Spain, 2018

ABSTRACT

Recessive Dystrophic Epidermolysis Bullosa (RDEB) is a severe skin disorder produced by a mutation in the COL7A1 gene (c.6527inC) and leads to dysfunctional or absent collagen type VII in the dermo-epidermal junction. Consequently, blisters appear throughout the body, including mucous membranes. Currently, diagnosis is routinely performed by rubbing the skin to induce a blister and taking a biopsy for histological analysis. Mutational analysis is possible but it is expensive and difficult. In this work, a suction device has been developed to substitute the current RDEB diagnostic method by a more precise, reproducible and reliable one. An easy to use device represents a less invasive method of diagnosis that betters the life of patients that may have severe conditions such as RDEB. The principal characteristics of the device are its small size and manageability. It is equipped with a vacuum pump for suctioning, connected to a pressure sensor, an OLED screen to provide real-time reading of the sensor, and an incandescent light bulb to provide heat. The device can be turned on and off by a simple pushbutton, and the suction modulated. It is operated by an Arduino-compatible microcontroller. To obtain the combination of pressure and time needed for blister generation, RDEB human skin mice models were developed using human plasma scaffolds as dermal component. Applying a negative pressure of 80-85 kPa for 5 minutes produced a well-defined blister at the DEJ, without damaging the dermis. Results were confirmed by Hematoxylin and Eosin staining and immunohistochemical studies of collagen VII, vimentin and cytokeratins 10 and 14. Temperature influenced blister generation. Higher negative pressures proved to cause dermal disruption, with DEJ and intradermal blistering, as well as tissue deformation. Epidermis remained intact in all cases. To complement this work and explore one of the possible applications of the device, the result was tested on a skin model corrected for the COL7A1 gene mutation that was provided by another research group. Collagen VII was observed, and tissue architecture was conserved after suction without dermal disruption or blisters. In conclusion, determining blistering times for EB represents a great advance in the diagnosis of the disorder. Helping such patients determine their condition may greatly influence their cures. In addition, the data obtained may help in develop specific treatments for the different types and subtypes of RB, including RDEB.

ACKNOWLEDGEMENTS

First and foremost, I would like to thank my tutor, Marta who has patiently taught me everything she could during this process and helped me achieve personal and professional goals. Also, Fran, who gave his time and knowledge, without him this project would not have been possible.

My parents, who have put up with my nonsense every day and kept me going until the end. Thank you for understanding and supporting my decisions, and thank you in advance for everything you will do for me in this new period.

Finally, I have to mention my friends, for all the rants, desperations, laughs, cries, trips, and meaningful moments that we have been through and still have.

«Para mi abuela, mi mayor fan, que siempre confió en mí. Descansa.»

CONTENTS

LIST OF FIGURES

LIST OF TABLES

1. INTRODUCTION

1.1. Motivation and Objectives

The diagnosis of Epidermolysis bullosa is standardly performed taking a biopsy of a freshly induced blister in the patient, generated by rubbing the skin, and analysis using immunohistochemical methods and electron microscopy. Mutational analysis can be performed to make an exact diagnosis, but it is expensive and not easily accessed. This project arose from the need for a more accurate and standardized method for generating blisters in a controlled manner that could be reproducible and available for clinical use.

In this work, the plan was to develop a method of diagnosis by exerting a vacuum force on the skin and creating a blister by means of a simple device. This was created with the functionalities needed for the diagnosis of EB, and in a shape and size for it to be manageable and easy to carry. An apparatus with good characteristics was found, and the casing was taken from it, while the other elements would be introduced and modified to achieve the final product.

In order to test the parameters of blister generation, an *in vivo* experiment was designed, with human skin grafts developed in culture and transplanted into immunodeficient mice. To confirm the hypothesis, in addition to visual proof, histological and immunohistochemical analyses were made.

1.2. Background

1.2.1. The Skin

The skin is the largest organ in the human body, accounting for almost 2 m^2 of its surface and up to 20 % of its total weight, with variable thickness throughout. Also known as the integument, its functions include protection, support, regulation, communication and synthesis. It provides a physical barrier against mechanical and thermal damage, as well as being selectively permeable and balancing the water homeostasis. Additionally, it protects the body from pathogens like microorganisms and other substances and initiates the immune response whenever these go through. The skin has many different sensory receptors all over the body, to detect changes in the environment and regulate the body accordingly. More specifically, this organ has several thermoregulation mechanisms to maintain a constant temperature. Furthermore, the skin has metabolic functions such as excretion of excess metabolites, vitamin D synthesis, and energy

storage [1]. A simplified representation of the main structures of this organ can be seen in Figure 1.

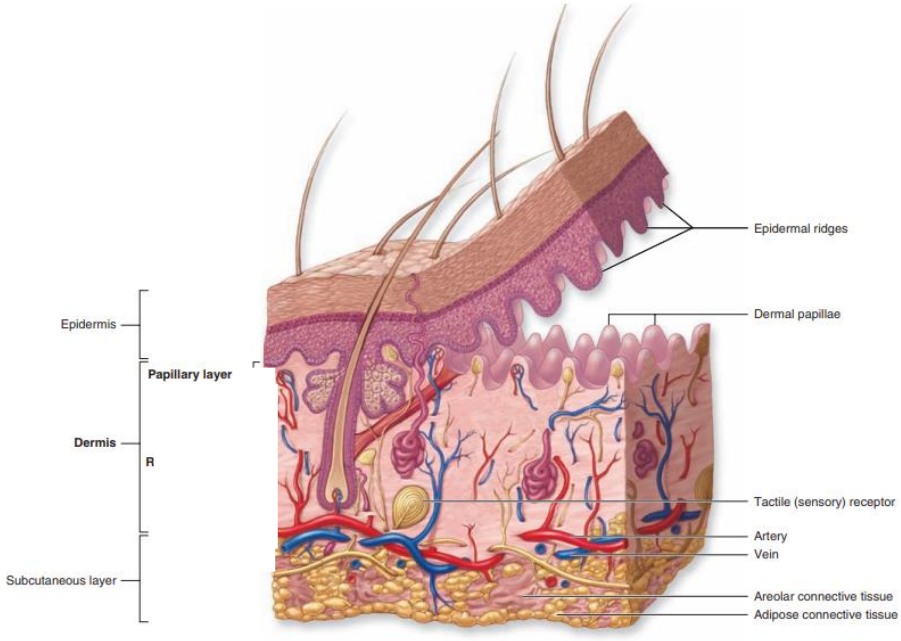

Figure 1: *Schematic representation of the skin showing major layers, representative structures and vascularization. Hair follicles are present from the dermis up to the outermost layer, as well as glands and sensory receptors. Along the junction between the dermis and epidermis, two structures can be identified: epidermal ridges and dermal papillae. Their function is to strengthen the union.* [1]

The skin requires basic features that are present in almost every tissue. The mechanical strength necessary is provided by an extracellular matrix, which is secreted by the cells in the tissue. To obtain nutrients and oxygen, as well as removing waste products, a network of blood and lymphatic vessels is needed. These vessels also protect the tissue against infections by providing access to the immune system. Additionally, nerve fibers are present to carry information from the sensory receptors of the tissue to the central nervous system, and to deliver signals for muscle contraction or glandular secretion [2].

The skin consists of two types of tissue: epithelia, corresponding to the epidermis, and connective tissue, corresponding to the dermis and subcutaneous layer.

a) Epidermis

The epidermis is the most external layer of the skin, in contact with the environment. It is a stratified squamous keratinized epithelium composed of keratinocytes. Their name comes from their characteristic keratin intermediate filaments, which contribute to the tissue's strength. These cells do not produce extracellular matrix and are tightly bound

together by a variety of cellular mechanisms. The epithelium does not contain blood vessels, lymphatic vessels or nerve fibers, so it needs a supporting tissue to nourish it (connective tissue), as well as efficient communications and diffusion mechanisms between cells.

The epidermis has several layers or stratums (Figure 2), characterized by the shape of the cells and their stages of differentiation on each of them. The innermost layer, or *basal*, is composed of cuboidal or columnar cells set on top of the basement membrane. This structure is a thin, organized layer of extracellular matrix, secreted by the dermis' cells, underlying epithelia. It has adhesive, filtering and barrier properties, and limits the epidermis from the dermis. The basal stratum is characterized by keratinocytes with high mitotic activity and presence of progenitor cells (adult stem cells) to regenerate the tissue. In humans, this regeneration occurs every 15 to 30 days, depending on the age and location in the body. The next stratum is the *spinous* layer, with polyhedral cells that make up for the most part if the epidermis, especially on the epidermal ridges (Figure 1, Figure 2).

The *granular* layer is composed of flattened cells tightly sealed together, with their characteristic keratohyalin granules, grains composed of keratins and histidin-rich proteins. Keratinocytes of the granular and upper spinous layers have lamellar granules, that liberate lipidic substances to create a hydrophobic coat on the membrane and block penetration of external substances. Cells in this layer are in the final stages of differentiation, going through the keratinization process.

Finally, the two outermost layers, *stratum lucidum* and *stratum corneum*, consist of flattened cells that have lost almost or all their organelles and nucleus. Their cytoplasm is filled with a mesh of keratin filaments and other cross-linked proteins (involucrin, loricrin, and others), and they are shed at the skin surface. Stratum lucidum is only found in thick skin, while stratum corneum is present in the whole body surface [1], [2], [3].

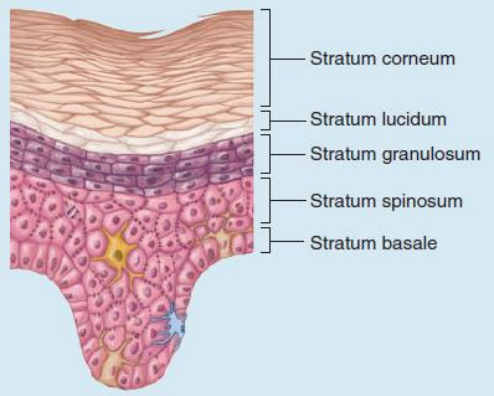

Figure 2: *Diagram representing the epidermis and its layers.* [1]

An important feature of this tissue is the intracellular adhesion. There are several structures that maintain tissue integrity by joining and communicating epidermal cells. *Tight junctions* seal adjacent cells laterally by two transmembrane proteins, claudin and ocludin, reinforcing the epidermis' selective permeability by ensuring molecules only pass the tissue through the cells. *Adherent junctions* bind the cells similarly through cadherins, attached to the cytoskeleton. Both structures encircle the apical ends of epithelial cells. *Desmosomes* are spot junctions in a circular shape that appear in the cytoplasmic side of each cell's membrane. Cadherins connect the two plaque-like structures (composed mainly of desmoplakin and plakoglobin), that are anchored to the IF. *Hemidesmosomes* look similar, except they join the cell to the basal membrane, by means of mostly integrins that bind extracellular proteins. Finally, *gap junctions* are adhesions that double as communication paths between cells. Transmembrane proteins, connexins, aggregate into circular patches in the plasma membrane, forming small hydrophilic pores for intercellular exchange of molecules [1].

- **Keratins, Intermediate Filaments and Keratinization in the Epidermis**

  Intermediate Filaments (IF) are chemically stable, long and unbranched components of the cytoskeleton in cells. These structures have a high cell-type specific protein composition, and keratins are the IF proteins of the epithelial tissue. They span through the cytoplasm and attach to the characteristic cell-cell adhesion structures in the tissue: desmosomes and hemidesmosomes [4]. Keratin IFs provide mechanical stability and structure to the cells and tissue (cell-cell junctions and adhesion to basement membrane), as well as certain signaling functions. Keratins have been classified according to the chromosomal site of their encoding genes into types I and II [5]. During epidermal differentiation, keratinocytes move upward, transitioning from

the proliferative basal layer to the post mitotic suprabasal layers, undergoing the keratinization process. The types of keratin filaments and their expression changes up to the superficial cells, in which keratins are half of the total protein mass. In the basal layer, IFs composed of K5/K14 IF bundles are predominant along the undifferentiated basal keratinocytes and are also present in further differentiation stages along the lower suprabasal epidermal layers. K1 and K10 are the major proteins in keratinocyte differentiation and keratinization and form denser bundles along the suprabasal layers (spinous, granular, stratum corneum). They are involved in structural stability and mechanical strength as well as other functions such as inhibition of keratinocyte proliferation by K10 [6].

b) Dermis

The dermis consists of two non-delimited sublayers of simple connective tissue below the epidermis. This type of tissue is composed of non-polarized cells, fibroblasts, immerse in extracellular matrix (ECM). These cells are in charge of secretion of collagen and elastin, main components of the connective tissue ECM. The dermis carries blood and lymph vessels and nerves, and provides structural support to the epidermis (Figure 3). The extracellular matrix includes a collagen and elastic network and a ground substance of carbohydrates and proteins (glycosaminoglycans, proteoglycans and other adhesive glycoproteins). The large complex molecules of the ground substance osmotically attract water to the tissue resulting in swelling (turgor). Pressure from turgor helps the ECM resist compressive forces [7]. The collagen fibers present in the dermis are many, but the most abundant are type I, III and V. Other collagen types influence the network's characteristics, according to the specific intra-tissue localizations.

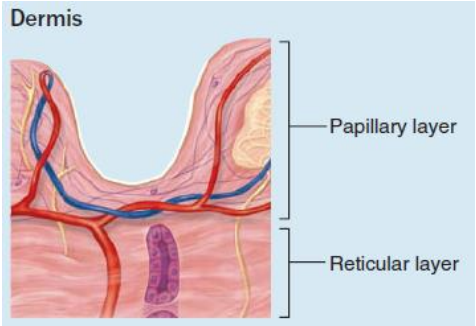

***Figure 3**: Diagram representing the dermis and its layers.* [1]

The contact surface with the epidermis is uneven and characterized by the presence of dermal papillae (Figure 1), opposite to the epidermal ridges. Its thickness depends on the area of the body, and can reach a maximum of 4 mm. The uppermost layer is called papillary layer, and is made of loose connective tissue, including types I and III collagen fibers. The cells present in this area are fibroblasts and scattered mast cells, macrophages, and other leukocytes. Additionally, collagen VII anchoring fibers insert into the basement membrane and join the two tissues. The reticular layer of the dermis is a thicker dense connective tissue area, with mainly type I collagen [1], [7].

c) Dermal-Epidermal Junction

Skin integrity is guaranteed by the appropriate attachment of the epidermis to the dermis. The Dermal-Epidermal Junction (DEJ) plays a crucial role as an anchoring site of both tissues. It can be considered as four units, characterized by the expression of different protein components. These units are included within the epidermal cells, the basement membrane, and the dermis.

The basement membrane (BM) is a sheet of extracellular matrix composed of glycoproteins. The upper layer, closer to the epidermis and secreted by its cells, is called *lamina lucida*. Below, the *lamina densa* is the layer produced by dermal cells. The functions of the BM are diverse. It provides structural support and polarity to basal epithelial cells and attaches them to the dermis. In addition, it affects epithelial cell membrane organization, as well as mediating their interactions and migration. It also filters and accumulates substances from the dermis to the epidermis.

A schematic diagram of the proteins involved in the DEJ and their location within the tissues is shown in Figure 4.

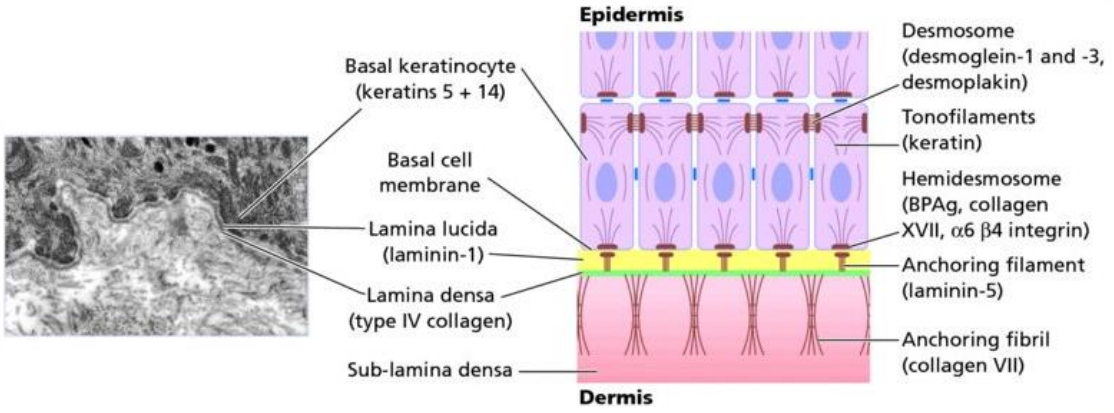

Figure 4: *Dermal-Epidermal Junction. Schematic representation corelated to a histological image of the skin. Four domains of DEJ: basal cell layer, lamina lucida, lamina densa, sub-lamina densa. Main components in this structure and the related proteins are listed (desmosomes, hemidesmosomes, anchoring filaments and fibrils).* [8]

First, the structure within the basal keratinocytes that binds them, and the epidermis, to the dermis is the *hemidesmosome*. This structure is composed of intracellular and transmembrane proteins. Plectin, an intracellular protein, connects keratin intermediate filaments (K5/K14 bundles) to transmembrane integrins (α6β4) and collagen XVII fibers. Through the lamina lucida, laminins (332) bind hemidesmosomes to collagen IV in the lamina densa. Underneath the lamina densa, collagen types III and VII in the anchorin fibrils secure this structure to the dermal network. Moreover, there is another protein complex that plays a role in DEJ, at the interface between the basal keratinocyte layer and lamina lucida. Kindlin-1, complemented with integrin α3β1, joins intracellular filaments of actin to a laminin in the lamina lucida.

1.2.2. Inherited Epidermolysis Bullosa

Epidermolysis bullosa (EB) refers to a group of diverse genetic disorders in a variety of structural proteins of the skin, that fall into the category of mechanobullous genodermatoses. The variants of 20 genes have been known to cause the different types and subtypes of EB [9]. As a result of said mutations, these disorders can involve alterations such as simple molecular defects or lack of key adhesion proteins. The characteristic phenotypes are variable, and range from tissue fragility on mechanically exposed sites as hands and feet, to formation of blisters and wounds such as those seen in Figure 5, all in response to mechanical trauma [10]. The genes involved are expressed in other epithelia of the body, such as the gastrointestinal, urinary, respiratory or skeletal systems.

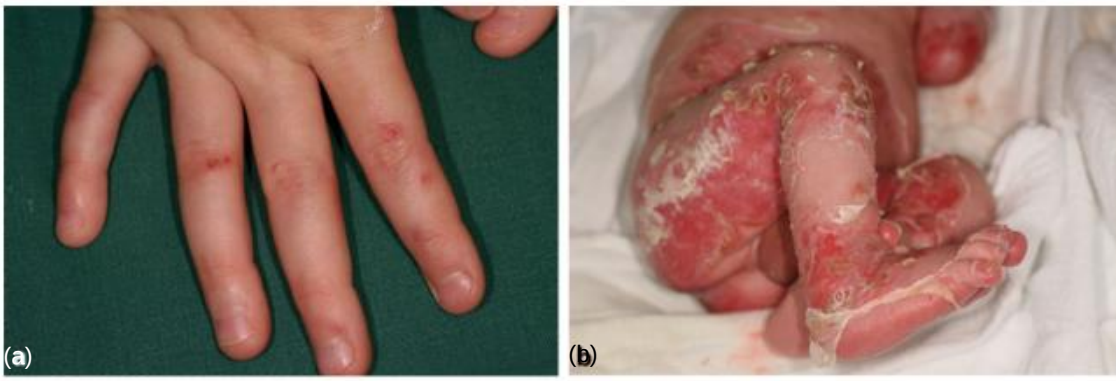

Figure 5: *Epidermolysis bullosa phenotypes. The disease can have diverse effects. (a) Localized blistering and erosions on skin exposed to mechanical forces (hands, feet). (b) Generalized blisters, erosions and exposed skin all over the body, lethal type of epidermolysis.* [11]

The incidence of this disease is approximately half a million patients worldwide [12], and according to the Orphanet database, the prevalence of this disease is of 1-9 over a million [13]. In the United States, the incidence is of nearly 1/53000 live births, and 1/125000 of prevalence –with similar data in several European countries. According to this, EB is considered as a rare disease (RD), which affect only small numbers of individuals (5 out of every 10000 or less) [14]. The issue with these conditions is that, due to the low incidences and the complex origins, the research dedicated to them is scarce and scattered throughout different countries. Consequently, there are few specific health policies dedicated to them, and diagnosis is difficulted, as well as access to treatment or care.

The classification of the diverse types of EB has been changing throughout the years since it was first reported with such name in 1886. Along with the discovery of new technologies and techniques, the data available kept bringing light into what were the underlying causes of the symptoms observed. At first, the focus was on distinguishing between the inherited and acquired forms of EB, and later on the three major types were established – simplex, junctional and dystrophic. This first classification was based on the degree of tissue separation observed. The development of immunofluorescence techniques and other protein analysis methods allowed for the detection of certain molecules involved in EB, along with a proper diagnosis.

The progress in genetics of the 1990s (DNA sequencing, gene mapping and cloning) enabled the discovery of the underlying mutations causing these molecular malfunctions [15]. From that, mostly subtypes of EB were identified, and other genodermatoses were included, such as Kindler syndrome. The progress was reported in the *International Consensus Meetings on Diagnosis and Classification of Epidermolysis bullosa*, the last

one to date being the third in 2008 [16]. Although the classification has progressed significantly, even more mutated genes, mutation mechanisms and phenotypes are emerging.

Four types of EB are distinguished within the allelic heterogeneity of the disease, each characterized by the location and protein causing the cleavage in the skin, shown in Figure 6. Epidermolysis bullosa *Simplex* (EBS), with intraepidermal cleavage; *Junctional* (EBJ), where the skin breaks in the lamina lucida of the basement membrane; *Dystrophic* (RDEB) with breakage below the basement membrane (anchoring fibrils); and *Kindler syndrome* (KS), with variable location of cleavage. Furthermore, EB types are identified according to other criteria such as clinical severity, inheritance pattern (dominant or recessive), relative protein expression and type of gene mutation [9].

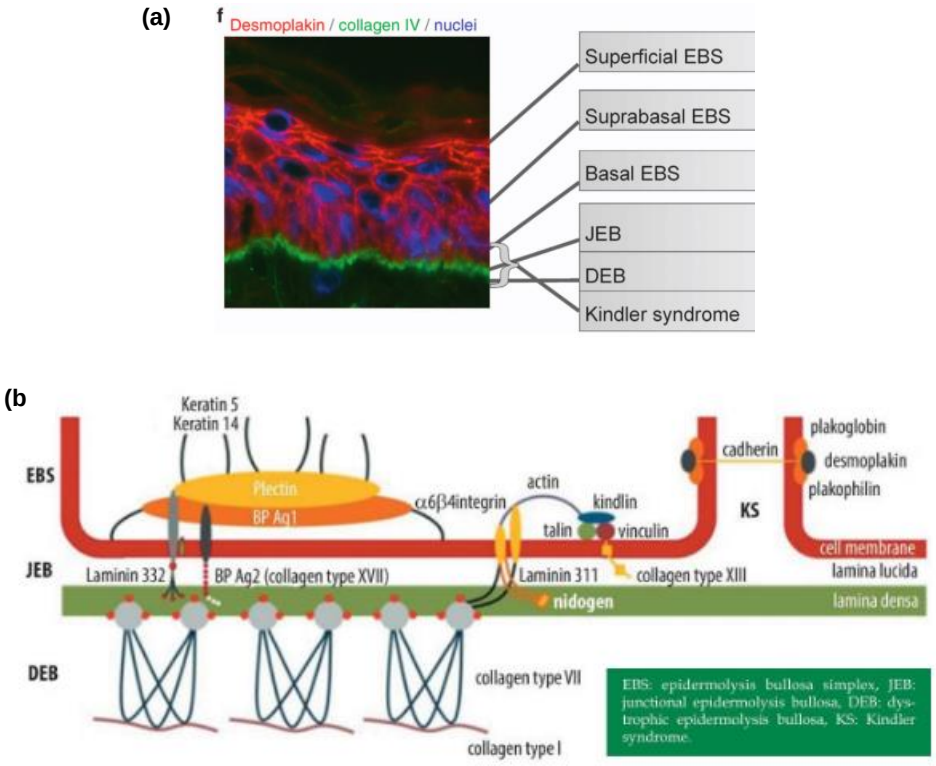

Figure 6: *(a)Immunofluorescence staining of normal human skin with antibodies to demsoplakin, collagen VII and nuclei and EB types indicating their respective levels of breakage.* [15] *(b) Representation of the proteins affected in different types of inherited epidermolysis bullosa.* [17]

- ***Epidermolysis bullosa Simplex (EBS)*** affects the epidermal layer. It is the most common type and it is inherited in an autosomal dominant manner. Two EBS groups can be distinguished, depending on where on the epidermis the mutated protein is mostly expressed. Suprabasal EBS affects proteins within cell-cell adhesions such as desmosomal plakoglobin or desmoplakin. The disorder does

not manifest with clear blisters, but with erosions or increased desquamation due to fragility of keratinized cells. Basal EBS is mostly caused by mutations on the keratin 5 and 14 encoding genes. Hence, the cells are partially or completely unable to form keratin intermediate filaments, and cytoskeleton destabilization and cytolysis occur.

- On ***Junctional Epidermolysis bullosa (JEB)*** the blistering appears on the lamina lucida, and it is normally inherited as autosomal recessive. Localized and generalized subtypes can be distinguished. Herlitz JEB is a generalized variant that affects laminin-332, with blistering on extensive mucocutaneous surfaces present from birth. The mortality rate is 100% on the first years of life, due to severe complications such as pneumonia, airway obstruction and sepsis. Other subtypes (Generalized intermediate JEB) present high risk of squamous cell carcinoma.
- ***Dystrophic Epidermolysis bullosa (DEB)*** appears with mutations on the COL7A1, coding for collagen VII, and it is inherited as autosomal dominant or recessive. These mutations affect the structural integrity of anchoring fibrils, so the blistering appears between the dermis and epidermis, below the basement membrane. In severe cases, complete protein loss occurs, with extreme skin fragility, scarring, mutilations, malnutrition or growth retardation as disease complications.
- ***Kindler syndrome (KS)*** is a genodermatosis included in the EB groups, characterized by the mutation of the gene FERMT1, which codes for kindlin-1. This protein anchors basal keratinocytes to the actin filaments of the cytoskeleton. KS causes blisters in childhood, as well as other complications skin atrophy, photosensitivity, gingivitis, periodontitis, and other urogenital and gastrointestinal issues. Moreover, nonmelanocytic skin tumors can appear in KS patients.

For further reference, all known types and subtypes of EB are listed in ANNEX accompanied by their corresponding inheritance patterns, mutated genes and affected proteins.

In the following subsection Recessive Dystrophic Epidermolysis bullosa, the subtype employed in this work, is described in detail.

1.2.3. Recessive Dystrophic Epidermolysis Bullosa

a) Description

Recessive Dystrophic Epidermolysis bullosa is one of the two main subtypes of DEB, and one of the most severe EB types. It is caused by a recessively inherited mutation in the COL7A1 gene, which can lead to aberrant synthesis or defective assembly of Collagen type VII (C7). In consequence, anchoring fibrils in the dermal-epidermal junction partially or completely lose their adherent function. Due to the genotypical heterogeneity of mutations in COL7A1 gene, this disorder can give rise to many phenotypes and clinical manifestations.

Being recessively inherited, this disorder is characterized by the presence of mutations in both alleles of the gene, each inherited from one parent. These can be missense or nonsense mutations, combined between the two alleles, which explain the clinical variations observed within RDEB. The two most common subtypes are Generalized Severe (GS) and Generalized Other (GO). RDEB-GS appears when a premature termination codon mutation is present in both gene alleles, which gives rise to abnormally truncated polypeptides incapable of forming C7, that degrade inside the cell before forming anchoring fibrils. In RDEB-GO, one allele has a premature termination codon, while the other has a missense mutation. The cells are able to produce a somewhat functioning form of C7, structurally abnormal, that gives rise to a milder disease variety. In addition, other elements such as cytokines have been identified to affect RDEB phenotypes.

The clinical manifestations of RDEB-GS and GO are similar, the latter being milder as there is C7, even if not fully functional. RDEB manifests in the skin with mutilating scarring and blistering. Moreover, symptoms appear in mucous membranes, as esophageal strictures (leading to malnutrition and slowed growth), pseudosyndactly (fused fingers and toes due to progressive scarring), loss of nail plates, joint contractures, eye inflammation and visual impairment [18]. In addition, RDEB forms have been related to the development of squamous cell carcinoma (SCC) [19].

b) Diagnosis

Currently, the diagnosis of EB involves studying patient's history, course of the disease, and histopathology and electron microscopy examination, as well as a genetic study. The first step is to take a biopsy from a freshly induced blister in a clinically normal area of the patient's skin. Existent wounds do not ensure accurate results due to possible re-epithelialization under blister roof and degradation of important proteins during

inflammatory immune response. The skin is rubbed applying torsion with a pencil eraser or until the area turns red, and the punch biopsy is taken. For less severe EB patients such as EBS or dominant DEB, prolonged (up to 3 hours) torsion force may be required for inducing a new blister [20].

Transmission Electron Microscopy (EM) is considered the gold standard laboratory test for differentiation between the various forms of EB. This technique provides means for visualization of ultra-structural abnormalities and gives semi-quantitative information about structural deficits. For EBS or DEB, where issues may arise from morphological abnormalities in intermediate filaments, EM may be particularly useful to detect abnormalities that immunohistochemical analyses cannot detect. Nevertheless, EM is an expensive and time-consuming technique, and nowadays not so many laboratories can provide accurate results, as it requires an extensive training period.

Immunohistochemistry offers a diagnostic with comparable precision to EM. It is simpler, more convenient and faster both to perform and to interpret, and less expensive. With the use of specific monoclonal antibodies, it can provide information about the most likely mutated structural protein as well as the EB type [21].

However, the most effective method for detection of the inherited gene defect(s) is mutational analysis. It allows to predict clinical severity, phenotype, and natural history of the disease, as well as the mode of inheritance and chances of recurrence in offspring. Techniques for mutational analysis include Next Generation Sequencing (NGS), genotyping of Sanger sequencing for known mutations, variants or even genes (as COL7A1); multigene panel testing, RNAseq, PCR in cases where no specific information is available; and whole exome or genome sequencing [9].

c) Treatment

Nowadays, this disorder can be managed with multidisciplinary palliative wound care and trauma minimization, complemented with support groups such as *DEBRA (Dystrophic Epidermolysis Bullosa Research Association).* In addition, due to the high risk of SCC, skin cancer screenings must be regularly performed on the patient.

However, many therapies are being researched and developed with promising results, not yet brought to the clinical application. For information about ongoing clinical trials, there are many up to date references such as *Clinicaltrials.gov* from the United States National Library of Medicine or the *European Union Clinical Trials Register*.

Some of the most significative therapies are briefly explained in the following lines:

- **Gene therapy** consists on correcting the altered genome by transferring a functional version through a viral vector. The target must be stem cells (in the case of EB epidermal stem cells), for the tissue to develop correctly after renovation. The newly functional cells are grafted into a fresh wound in the tissue as call sheets or skin equivalents. Gene therapy presents two major drawbacks. First, the skin regeneration is difficult in certain body parts, such as mucous membranes or gastrointestinal surfaces. Second, there is a chance of developing an immune reaction to the collagen produced by genetically corrected cells, especially in RDEB forms where C7 is not present at all [18]. Additionally, the risk of adverse mutagenic effects increases with the use of vectors capable of long-term gene expression, adding on to the risk of SCC that RDEB patients have.

  Gene editing mechanisms use site-specific molecule complexed to cleave the DNA helix and introduce the desired genetic code in the generated space. CRISPR/Cas9 is a two-component system composed of a nuclease (Cas9) that conjugates with a small RNA transcript (gRNA) that serves as a guide. This complex targets a complementary DNA sequence consisting of 15–20 nucleotides. Once the desired DNA break is generated, genome modification by homology-directed repair (HDR) is done, precisely inserting donor DNA into the targeted site. It allows for specific, efficient gene editing with possible *in* vivo applications [22].

  Revertant mosaicism is a «natural gene therapy» mechanism found in several organisms, where the disease-causing mutation is locally corrected. This happens through postzygotic somatic molecular events such as second-site mutations or homologous recombination. Initially, it was thought to be a rare occurrence, but in EB it has been reported in all types in different genes [23].

- **Fibroblast cell therapy** consists on injecting the patient with fibroblasts from healthy donors intradermally. This treatment has been demonstrated to have several months of duration in which partially functional anchoring fibrils are present [24]. It is suitable for milder disorder manifestations.
- **Mesenchymal stem cell (MSC) therapy** is based on intravenous or intradermal injections of these cells into EB patients. Benefits have been reported in several clinical trials –with children and adults– including better wound healing, decreased blistering, less skin pain, or presence of functional anchoring fibrils. However, the mechanisms of action of MSCs are yet to be determined. It is probable that their capabilities of mediating immunosuppressive and immunoregulatory effects are the cause for patient improvement, rather than the

de novo synthesis of C7. When grafted into HLA-compatible patients, the likelihood of graft versus host disease and other immune responses is low. Furthermore, the possibility of targeting endogenous MSCs with gene therapy is being researched, to allow the body to produce progenitors capable of proper wound healing [25].

Cell therapy and gene editing procedures can be combined to give rise to genetically corrected autologous cells to be implanted or injected in the patient for long-time restoration of function. An example of such therapy can be seen in [26].

- Another future treatment is **protein therapy**. Injecting intradermally purified C7 human protein into RDEB mice models has been proven successful, with anchoring fibril formation and consequent enhanced dermoepidermal adherence. For more generalized cases, intravenous injections can be done. Some drawbacks exist to this treatment method. Due to degradation of the protein, repeat injections would be needed after a certain amount of time. Also, the immune response to foreign C7 is yet to be determined [18].

1.2.4. Plasma as a Dermal Scaffold for Skin Grafts

The skin grafts used for transplant in this project were generated in cell culture using human plasma as the dermal component.

Bioengineered skin grafts have been developed for treatment of skin diseases and applied to different fields. They can be introduced to restore burnt or ulcerated tissue, created to locally or systemically deliver therapeutics, or used as a realistic model to replace animal-based tests in drug development or toxicological assessment. Modeling skin diseases in a humanized context is crucial for understanding disease mechanisms. In addition, disease modeling *in vivo* enables preclinical studies potentially positive for the clinical outcome. For this purpose, cells obtained from skin biopsies can be expanded *in vitro* and assembled in three-dimensional matrices to develop skin equivalents (Figure 7).

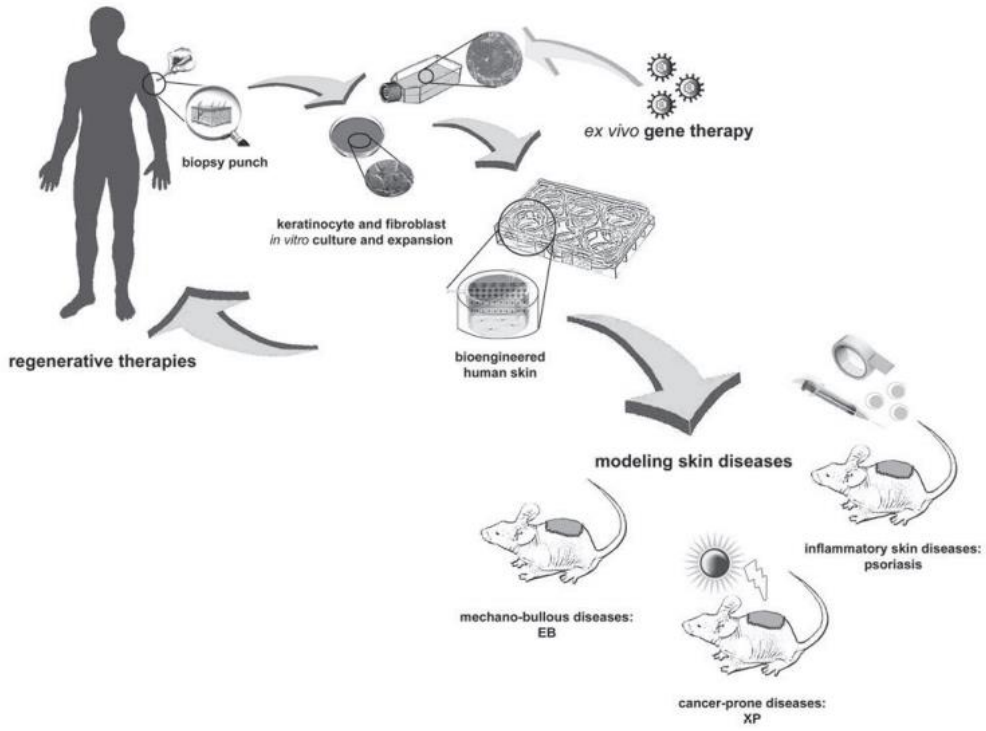

Figure 7: *Simplified representation of generation of disease human skin models in vivo* [27].

Previous works ([27], [28], [29]) have developed a method for successful skin model generation and grafting onto the back of immunodeficient mice. Skin of human origin is regenerated, vascularized and innervated by mouse vessels and nerves. The result was healthy and mature skin preserving human tissue architecture that persisted after several epidermal turn-overs, demonstrated by immunohistochemical assays during follow-up periods. Human keratinocytes and/or fibroblasts are selected from the patient to replicate the desired conditions. In addition, cells can be genetically manipulated to express or silence preferred genes, generating transgenic or KO humanized-skin respectively. Gene therapy approaches in combination with the bioengineered skin humanized mouse model constitute a robust platform to conduct preclinical studies.

1.2.5. Suction Device

The final product was developed from an already existing apparatus, to conserve its shape and manageability. The original appearance can be seen in Figure 8. This device functioned discretely and had no control unit to regulate its operation mode.

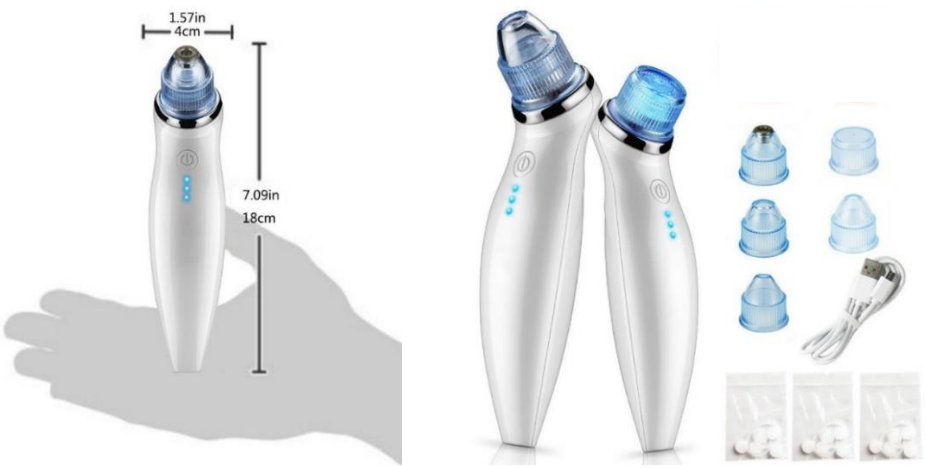

Figure 8: *Original device. Blackhead remover from brand Beauty Nymph. Amazon.es*

To modify the device, the most essential step was including the Arduino Nano controller, which can be later programmed to provide all the functionalities needed. The element that exerts the force is a vacuum pump, and to control its intensity, a potentiometer is used. To turn the device on and off, a push button was introduced, with a connection to a digital input in the Arduino. The project is based on exerting pressure on the skin to generate blisters, so knowing how much the device is applying is crucial. For that, a sensor was included, to read this parameter directly from the outlet of the pump. In order to see the data while using the device, there is a small OLED screen attached to it, that shows the reading of the pressure sensor. In addition, an incandescent light bulb was introduced, which produces heat. This functionality aids in the formation of the blister. The block diagram in Figure 9 represents in a simple manner the main components and functions of the device.

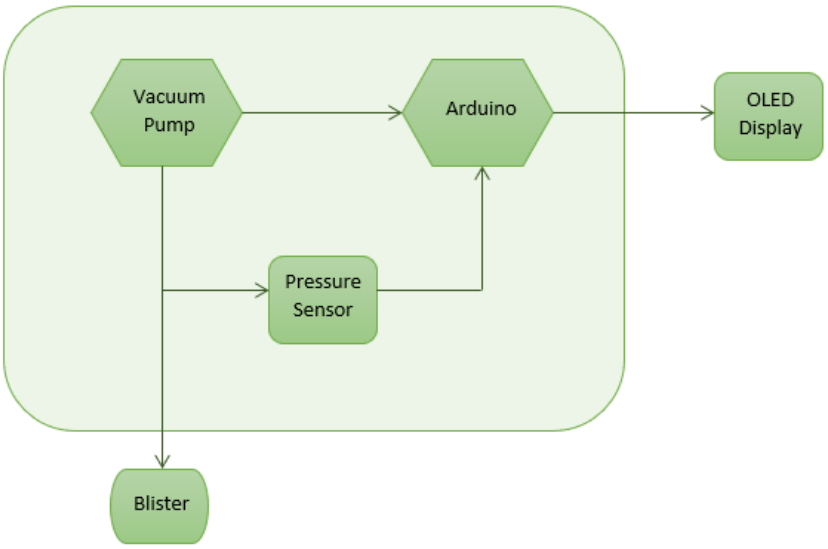

***Figure 9**: Block diagram of the device's functioning. Only the main components are represented: the vacuum pump to generate the blister, and the microcontroller that receives the data form the sensor and shows it in the screen.*

The device was modified to have the following elements: Arduino-compatible microcontroller, vacuum pump, pressure sensor, pushbutton, resistors, OLED display, incandescent light bulb, transistors, capacitor and diode.

A brief explanation of the basic functions of every component used to build the device is offered in the following subsections.

a) Arduino-Compatible Microcontroller

Arduino is a platform that allows the development of a broad range of electronic projects based on an open-source software and hardware modules or boards [30]. It is a microcontroller that, through a programming language, allows for communication between the computer and the environment. Said language is composed of a set of functions in C/C++ that pass through a compiler (*avr-g++)* to be translated into machine readable instructions.

For this project a board compatible with Arduino Nano V3.0 was used (Figure 10), with the CH340G USB chip instead of the official from Arduino. The programming is done through the official Arduino IDE. The main component is an 8-bit microcontroller ATmega328P, built by Atmel®, that is based on the AVR® architecture [31]. Because of the open-source nature of the Arduino hardware, and software, this device is fully compatible with and almost identical to an official Nano.

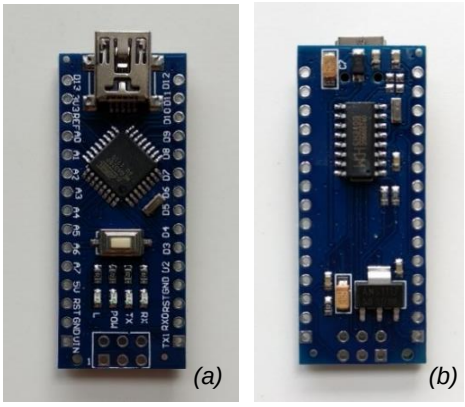

Figure 10 *Arduino Nano-compatible V3.0 board. (a): front, ATmega328P compiler. (b): back, unofficial CH340P USB chip (up) and ASM 1117 5V regulator (down).*

The boards contain a set of analog and digital pins that connect the circuit to the microcontroller. In addition, the microcontroller can communicate with the computer through a Mini-B USB connector, so that it can be programmed. In this way, it is possible to attach different types of electronic components to develop a multitude of projects.

In order to transform the input voltage to the 5 V that the device operates on, it has a voltage regulator (Figure 10 b). In the compatible board used it is the ASM 1117.

The technical specifications of this board are listed in Table 1.

Table 1: *Technical Specifications of Arduino-compatible microcontroller.*

Technical Specifications	
Microcontroller	ATmega328P
Operating Voltage	5 V
Input Voltage	7-12 V
Clock Speed	16 MHz
Analog IN Pins	8
Digital I/O Pins	14 (6 of which are PWM)
DC current per I/O pins	40 mA (I/O pins)
Flash Memory	32 KB of which 2 KB used by bootloader
SRAM	1 KB

EEPROM	1 KB
PCB Size	18 x 45 mm
Power Consumption	19 mA

The main advantage of this type of microcontroller is that both the software and hardware are user friendly but have the option of extension for more advanced users. The addition of functionalities in the software is done through collections of code, called libraries. Although the code is combined with the basic built-in libraries, it is possible to include other more or less complex, that can be official or third-party. The board is relatively inexpensive for the great quality and functionalities it provides.

b) Vacuum Pump

The vacuum pump is composed mainly of a sealed rigid chamber, an inlet, and outlet and a rotary shaft. When it is connected to a DC power source, the current creates a magnetic force that moves the shaft, displacing air molecules from the inlet to the chamber creating a partial vacuum inside. Air will then enter the pump to replace that vacuum, creating a negative pressure. The stages of vacuum generation in a typical rotary vane pump are shown in Figure 11.

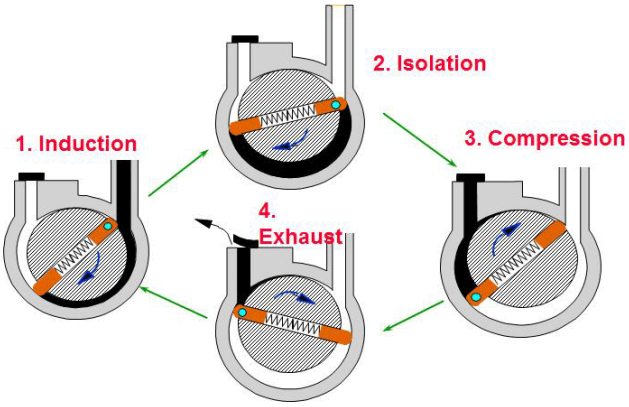

Figure 11: *Typical operation stages in a rotary vane pump. 1. Induction of gas into chamber. Pressure increases inside as a result if volume rise. 2. Isolation of gas inside the chamber. 3. Compression of gas due to reduction of space. 4.Exhausution.* [32]

The vacuum pump used in this work was that shown in Figure 12. The maximum vacuum (negative pressure) it provides is 250 mmHg (around 33.3 kPa), with 3 mmHg (0.4 kPa) of leakage. Its operating conditions range from 6 to 24 Volts and 0.42 to 0.12 Amperes respectively. At 12 V, the current draw is 280 mA.

Figure 12: *Vacuum pump LY370CPM.* [33]

c) Pressure Sensor MPX 4115A

It is an integrated silicon pressure sensor, with a piezoresistive transducer (Figure 13). These measuring devices are equipped with the sensing element, calibration circuitry and an amplifier. These elements are simplified in the schematic in Figure 14.

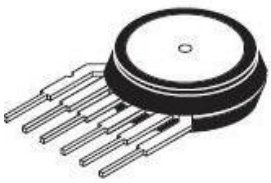

Figure 13: *MPX 4115A NXP Integrated Pressure Sensor.* [34]

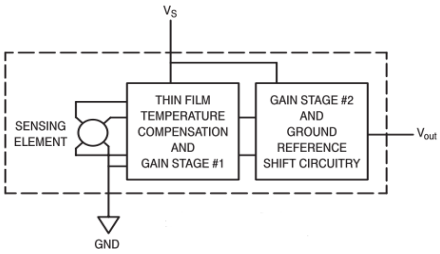

Figure 14: *Fully Integrated Pressure Sensor Schematic. [34]*

Because it is an integrated sensor, the output can be directly converted into ADC, without the need for an amplifier [35]. It provides an analog output signal proportional to the applied pressure that is being measured. The range of measured pressure is from 15 to 115 kPa, and the output voltage spans within 4.59 V. Moreover, this device has a good sensitivity of 46 mV/kPa. These and other characteristics of the sensor are listed in Table 2, taken from the sensor datasheet [34].

Table 2: *Operating Characteristics of the MPX4115A Sensor. Offset (V_{off}) is the output voltage at the minimum rated pressure. Full Scale Output (V_{FSO}) is defined as the output voltage at the maximum or full rated pressure. Full Scale Span (V_{FSS}) is the algebraic difference between the output voltage at full and minimum rated pressures. Accuracy (error budget) consists of the output deviation of parameters as linearity, temperature and pressure hysteresis, temperature span.*

Characteristic	Symbol	Min	Typical	Max	Unit
Pressure Range	P_{op}	15	-	115	kPa
Supply Voltage	V_s	4.85	5.1	5.35	V_{dc}
Supply Current	I_o	-	7.0	10	mA_{dc}
Minimum Pressure Offset	V_{off}	0.135	0.204	0.273	V_{dc}
Full Scale Output	V_{FSO}	4.725	4.794	4.863	V_{dc}
Full Scale Span	V_{FSS}	4.521	4.59	4.659	V_{dc}
Accuracy	-	-	-	±1.5	$\%V_{FSS}$
Sensitivity	V/P	-	46	-	mV/kPa
Response Time	t_R	-	1.0	-	ms
Offset Stability	-	-	±0.5	-	$\%V_{FSS}$
Maximum Pressure	P_{MAX}	-	-	400	kPa
Storage and Operating Temperature	T_{stg}, T_A	-40	-	+125	ºC

The value acquired from the analog reading of the sensor is transformed by the microcontroller into pressure. This is done using the transfer function (Figure 16) given in the datasheet [34], according to the Output versus Absolute Pressure graph shown in Figure 15. The final error in the pressure measurement is ±1.5, according to the data from Table 2: Operating Characteristics of the MPX4115A Sensor.

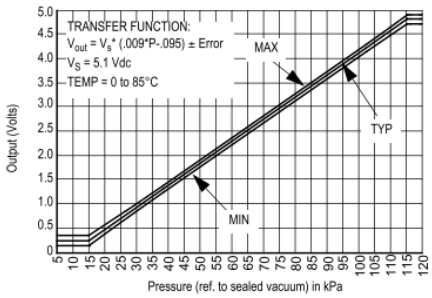

Figure 15: *Output vs Absolute Pressure of MPX4115A sensor.* [34]

$V_{out} = V_S (P \times 0.009 - 0.095)$
$\pm$ (Pressure Error x Temp. Factor x 0.009 x V_S)
$V_S = 5.1\ V \pm 0.25\ Vdc$

Figure 16: *Transfer function of MPX4115A sensor.* [34]

d) Pushbutton

A pushbutton is an electronic component that connects two points in a circuit when pressed [36]. The push button chosen was a standard one, with 4 pins.

e) Resistors

These components are placed in the circuit to cut or limit the flow of current, to create voltage reduction. To do so, they absorb energy, which is dissipated as heat. They are composed of a conductor material with a certain resistance measured in ohms (Ω). Resistors can play different roles in a circuit, for example, provide voltage control to transistors, protect components from excessive current, or act as pullup/pulldown resistors [37]. Moreover, another type are the variable resistors, also known as potentiometers, that can be set to deliver a certain fraction of the input voltage.

f) OLED Display

Monochrome OLED display with 128x64 pixels and 0.96 inches (Figure 17). The screen uses a SSD 1306 chip [38] that controls every pixel individually [39]. In addition, it is equipped with an I^2C interface that makes it very simple to control. This is a serial protocol interface that allows to connect to low-speed devices like microcontrollers and other systems. It is a simple mechanism that only needs two wires, Serial Data (SDA) and Serial Clock (SCL), with pullup resistors to connect any device equipped with I^2C [40]. Hence, the screen can be easily programmed with the Arduino IDE to display any data necessary.

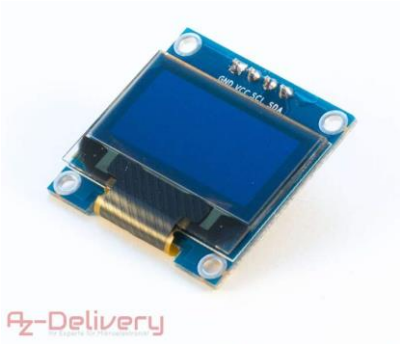

Figure 17: *0.96-inch I2C OLED display. az-delivery.de*

g) Incandescent Light bulb

It is an incandescent lamp, composed of a filament that emits light and heat when electric current passes through it. The filament is inside a sealed bulb filled with an inert gas or under vacuum, to prevent its oxidation [36]. The light bulb used for this project is shown in Figure 18.

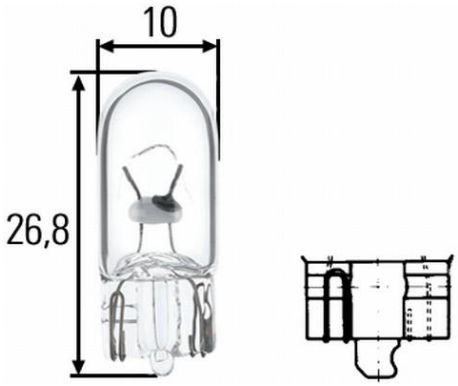

Figure 18: *Hella SWS light bulb.*
Technical specifications: 12 V and 5 W.

h) Transistors

A transistor is an electronic component made from semiconductor materials that has three connections (Emitter, Base, Collector). There are two basic types of transistors, Bipolar Junction Transistor (BJT) and Field-Effect Transistor (FET). In this project, BJTs are used. They are called “bipolar” because both holes and electrons act as current carriers. These devices can have two configurations, *npn* or *pnp*, which are illustrated in Figure 19 which operate similarly, except some features are reversed (polarity, current direction and functions of holes and electrons) [41].

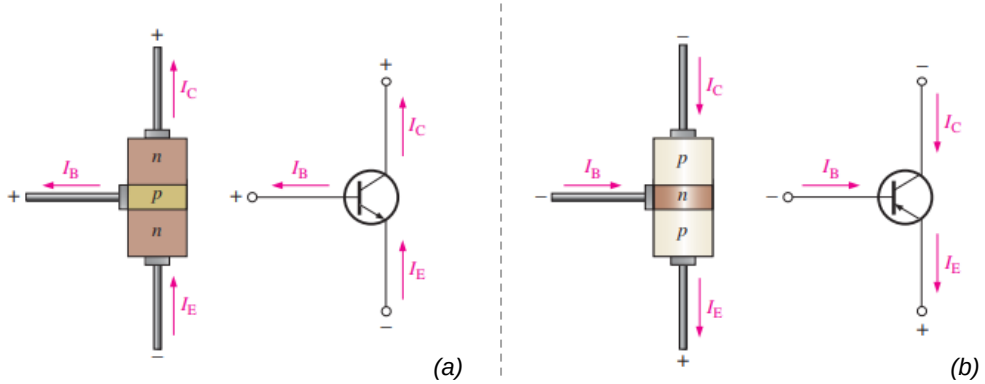

Figure 19: *Bipolar Junction Transistor. Two configurations shown: (a) npn, (b) pnp. Both operate similarly, except some features are reversed (polarity, current directions and functions of holes and electrons).* [41]

BJTs can be seen as a current input (through the base pin) and a current source (from the collector) to a circuit, dependent on said input. These devices have two different effects on electrical signals: amplification or switch operation. In the present work, both transistors have been used as switches, so this process will be further discussed. In switch mode, the transistor mainly shifts between two states, saturation and cutoff. In saturation, the current through the collector is maximum and does not depend on the base; and in cutoff mode, the transistor does not conduct between the collector and the emitter. For this purpose, a small current, such as those provided by the microcontroller pins, is enough to activate the switch function.

i) Capacitor

Capacitors are small electronic components that accumulate charge when connected to a power source and deliver it when disconnected. They are composed of two plates, one of them accumulates electrons when connected to the DC source, while repelling them in the other. As the power is cut off, the electrons migrate, creating a temporal current source [37]. The charging and discharging behavior of these components is exemplified in Figure 20.

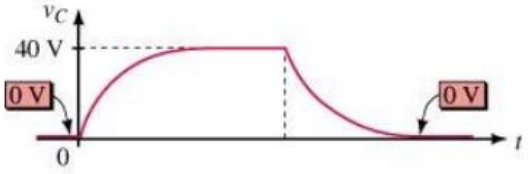

Figure 20: *Capacitor charge and discharge behavior* [42].

j) Diode

Diodes have two terminals, an anode and a cathode, and only allow current in one direction, when forward biased. This happens when the anode has a positive voltage that is higher than on the other end [37]. The applications may vary, and in this project, it is used to block the current from flowing in a certain way.

2. STATE OF THE ART

Suction-induced blisters have been studied as a useful tool to evaluate dermo-epidermal junction integrity. An early report from 1875 has been found where blisters where induced by cupping [43]. In the following years, other studies were developed [44]–[46] where cupping and direct vacuum were applied to the skin to observe skin separation with further histological assays. In addition, another skin split method has been reported that consists on separation by a sodium chloride solution [47].

Nowadays, suction split is used in research to generate standardized wound healing models, epidermal grafting, and other phenomena in the skin.

According to recent studies on blistering time on healthy skin patients [48], dermo epidermal adherence is influenced mostly, by skin temperature, and negative pressure plays a secondary role. Higher temperatures have been observed to decrease blistering time, as molecular processes leading to detachment or inflow of blister fluid seem to be enhanced. All in all, suction blistering time has been proven to be an indicator of DEJ adherence, as it provides information about the structural integrity of deeper subcutaneous layers.

A study from 1984 reported suction blister times measured for different types of EB in 16 patients with EBS [49]. The suction was applied with a suction cup connected to a vacuum pump delivering 200 mmHg (26.5 kPa) of negative pressure in different parts of the body (abdomen, arm, thigh and lower leg, corresponding to sites of predominant blistering). Temperature at blister site was measured after completion. The phenotypes included were: JEB (severe and non-lethal), dominant DEB (mild, moderate and severe) and RDEB (mild and severe). The results showed that mean blister times for all patients were around 80 minutes except for JEB subjects on whom the time for blister appearance was 10 minutes.

A different report compared salt split skin to suction split as a routinary method for differential diagnosis of two mechanobullous diseases [50]. The vacuum pump seen in Figure 21 was used to generate blisters at 300-350 mmHg (approximately 40-46 kPa) for 45 to 60 minutes in both normal and diseased skin. Biopsies were taken, as well as others for salt splitting, and analyzed by immunofluorescence. The results showed the presence of hemidesmosome proteins at the top of the blister, and basement membrane

components (collagens IV and VII, laminin) at the bottom. In addition, suction split was determined to be a more accurate, easier and faster diagnostic tool than salt split.

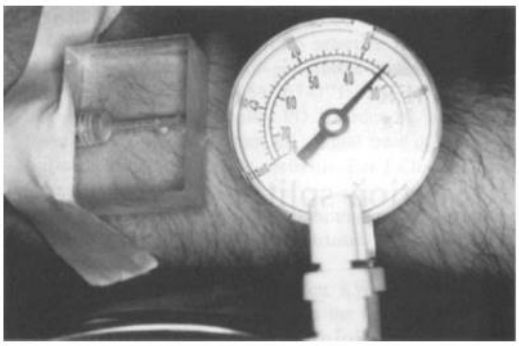

Figure 21: *Suction split apparatus. Hand vacuum composed of a plexiglass plate, with a terminal hole of 3 mm, and a pressure gauge, attached to perilesional areas.* [50]

In a clinical study for Potential of Systemic Allogeneic Mesenchymal Stromal Cell (MSC) Therapy for Children with Recessive Dystrophic Epidermolysis Bullosa [51]. Suction blisters were induced and times measured before and after MSC infusion using a negative pressure device (Electronic Diversities, MD, USA). The device is composed of a negative pressure source, connected to a suction chamber attached to the patient's skin. Inside the chamber, two light bulbs provide heat to the area. The pressure was set to 12–15 mmHg that produced a suction blister in a healthy person in 60 minutes. The mean blister times for the RDEB patients were of 10 minutes before any treatment (and reduced by 2 minutes after MSC infusion).

The most recent application of this method is currently being developed by researchers from Stanford University. Skin adherence for Recessive Dystrophic Epidermolysis bullosa (RDEB) patients is being measured [52]. The setup includes a suction blister device in a contact plate complemented with a heating ring and LEDs to illuminate target skin, connected to the corresponding power sources and to a laptop with a live imaging program. Reported results show that, at controlled conditions of negative 685 ± 30 mmHg (91 ± 4 kPa) and 37 ± 1 ºC, for healthy subjects 29.7 minutes are needed to generate a 1 mm wide blister, whereas for RDEB only 5.7 minutes were necessary. In conclusion, the device built is a useful tool to measure skin adherence at the DEJ, in a robust and quick way that can be implemented in clinical trials.

3. METHODS AND MATERIALS

The main procedures performed in this work were the fabrication of the suction device, and the *in vivo* experiment with the corresponding tissue analysis.

3.1. Device Assembly

In the previous section the device characteristics were explained, along with an overview of the functions of every component used in its fabrication.

The apparatus used as a model to build the actual suction device was composed of a vacuum pump, a button which changed through three intensities, and a connector to charge a battery inside it (Figure 8). The only components conserved were the pump and the mini USB connector.

The first step was to include the Arduino-compatible microcontroller. It is powered through the pin V_{in} with 12 V. As it is designated in the technical specifications of Table 1, the microcontroller works with 5 V, but the V_{in} pin was connected to the ASM 1117 voltage regulator which allows a maximum of 12 V input. The ground was connected to the voltage source.

The second most important component added was the vacuum pump (Figure 12). Its positive end was attached to the 12 V power source, in order to obtain maximum force. The negative end was connected to the collector of a npn transistor, a simple model TIP41. With the emitter of the transistor linked to ground, and the base to the microcontroller, it acts as a switch. From the D5 pin of the Arduino-compatible board the signal is sent so that the motor turns on with a certain intensity. This signal is a PWM (Pulse-Width Modulation), that works by modulating the duty cycle –“on time” or average between pulses– of a signal received [53], in this case from the potentiometer. The vacuum pump will receive a power supply equivalent to the mean of the time that the potentiometer has been at 0 and 5 V. In this way, it is possible to provide a continuous energy supply from two discrete signals. The potentiometer values are those form an analog signal transformed into 8-bit digital (discrete) values at the microcontroller analog pin (0-1023 range resolution). Through Equation 1: PWM transformation formula, the value from the potentiometer is converted into a pulse-width modulation signal to be sent to the motor. This equation is introduced to adjust the working range of the pump. Before, the potentiometer value span did not match the motor’s. This meant that the minimum

energy to overcome mechanical resistance and inertia of the motor's shaft was far higher than the minimum signal sent by the potentiometer. The PWM formula was introduced to adjust the signal sent to the motor to be able to use the whole value scope of the variable resistor.

Equation 1: *PWM transformation formula.*

$$\boldsymbol{PWM} = (\boldsymbol{potentiometer\ ADC} * \mathbf{0.21}) + \mathbf{40}$$

Therefore, the output is controlled, between 0 and 5 V, so that the transistor is able to undertake it. In addition, a 220 Ω resistor was included in the base to protect the transistor from excessive current. The intensity of the signal sent to the motor is controlled by a potentiometer, powered by 5 V, and linked to the A1 microcontroller pin.

The element that turns on and off the device is a simple standard pushbutton, with one end to the microcontroller 5 V provider pin, and the other to the D2 pin for reading the state of the pushbutton through the microcontroller. As the intention was to keep the on directive without having to continuously press the button, a pulldown resistor (220 Ω) was included between it and the ground. Therefore, when it is pressed once, the Arduino-compatible device receives the new state of the button, and initializes the whole device (including motor, light bulb, and pressure sensor). When pressed again, it stops.

Another essential component introduced was the pressure sensor MPX 4115A (Figure 13). It is supplied by 5 V, and the reading from it is delivered to the microcontroller to be transformed into pressure values through the analog pin A0. The sensor is connected directly to the pipe from where the pump draws air from the outside through a small fork-like part. One side was connected to the motor outlet, the other to the measurement component, and the last one to the device's outlet. Therefore, the measurements of the pressure in the outlet of the device (contact with the skin) can be taken as accurate, considering the error of the sensor (Table 2).

To complete the functionality of the device, a small 12 V light bulb was introduced. Controlled again by a transistor (BC547) acting as a switch –with a 220 Ω resistor to protect the base–, it was installed so that it turns on and off with the other components to a medium intensity (150 out of the digital scale of 0-255). Another resistor was added to protect the light bulb from excessive current.

Finally, the device fabrication was completed with the addition of the small OLED screen (Figure 17). As it was described in the previous section, the screen is equipped with an I^2C module, and it was connected to the board through the designated pins for this

purpose: pin A4 for SDA and A5 for SCL. The pullup resistors needed for these connections are provided by the microcontroller internally, which turn on automatically when the I^2C protocol is initialized [40]. To power it, it was linked to the 5 V and ground pins. Although the OLED display was designed for operating at 3 V, it is tolerant to 5 V, so it could be connected directly to the microcontroller board [39].

The device's circuit schematics were represented using the tool Eagle and can be seen in Figure 22.

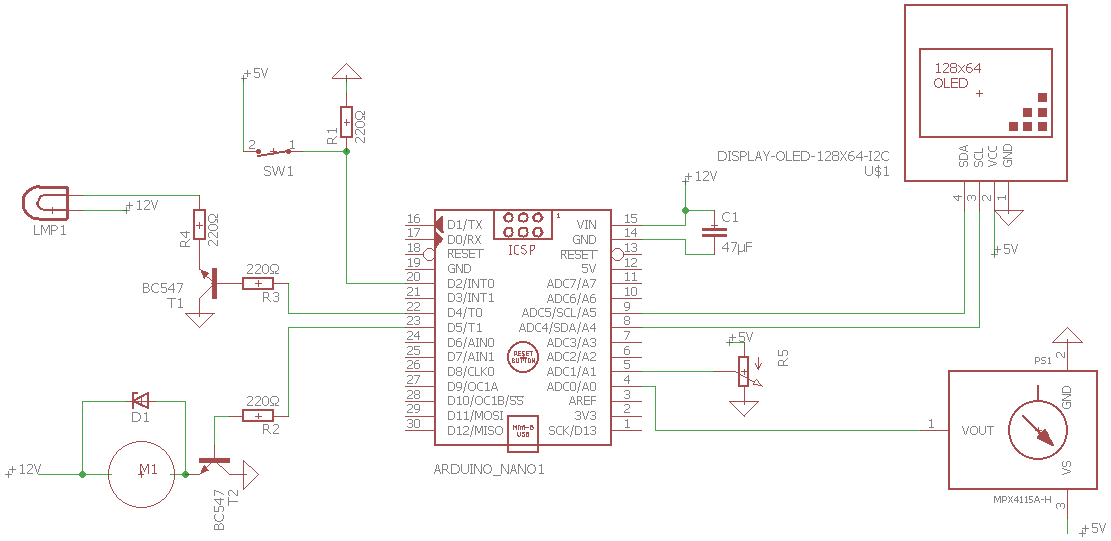

Figure 22: *Schematics of the circuit. In the middle, the Arduino-compatible microcontroller, along with a capacitor (C1) and a potentiometer (R5). On the right side of the figure, the OLED screen and the pressure sensor (PS1). On the left, the pushbutton (SW1), light bulb (LMP1) and vacuum pump (M). As well as these key elements, other components such as resistors (R1-4), transistors (T1-2) and a diode (D1) are introduced for optimization purposes.*

Regarding the power supply, the machine needs a 12 V for the vacuum pump, the Arduino-compatible board and the other components, which are provided by an external transformer (Salcar Electronics) through a mini USB connection to V_{in}. This pin in the microcontroller stands up to 12 V, according to the technical specifications in Table 1. The motor and light bulb draw power directly from this voltage source, as they need 12 V to function, and the other components are provided by the 5 V pin in the board. As for the current consumption, a raw estimate of the maximum needed was calculated in order to select the power source's characteristics. The microcontroller draws 24 mA when being powered by 12 V, and it can provide up to 200 mA through its pins. The vacuum pump consumes a maximum of 280 mA at 12 V. The pressure sensor consumes 10 mA, the OLED screen 20 mA, and the light bulb consumes 416 mA. This makes a total of 950

mA. Considering the other less consuming components, and to be safe, the current source chosen was of 3 A.

3.2. *In vivo* Model of Human Skin with Epidermolysis Bullosa

For this work, skin grafts using human plasma as a dermal scaffold were generated. To do so, fibroblast and keratinocyte primary cells were cultured. Then, artificial skin grafts were constructed following the specific protocol. Two models were generated, healthy (control), and diseased with both cell types taken form a patient with Recessive Dystrophic Epidermolysis bullosa (RDEB), carrying the c.6527inC mutation in COL7A1 gene [54], [55].

3.2.1. Cell Culture

Primary dermal RDEB fibroblasts and healthy cells were cultured in treated 75 ml ventilated flasks (F75) with Dulbecco's Modified Eagle Minimum Essential Medium (DMEM 1X) supplemented with 10 % Fetal Bovine Serum (FBS) and 1 % antibiotic to inhibit growth of contaminants. They were cultured in at 37 ºC in 95 % humidity and 5 % CO_2 conditions (Shel Lab $C0_2$ Serie; Sheldon Mfg. Inc incubator). Culture medium was replaced every 2 days with fresh media with the aid of the phenol red indicator [56]. Whenever confluence was reached, passages to subcultures were done to ensure proliferation and avoid senescence. The detachment of cells was done by trypsinization. After removing the medium, the cells were incubated with trypsin. The trypsin was then neutralized with medium, to avoid cytotoxic effects, and the sample was centrifuged for 7 minutes at 1000 rpm. Finally, the pellet was resuspended, and the cells seeded in the flask.

Primary human keratinocytes were obtained from skin biopsies of healthy and RDEB donors by enzymatic digestion according to previously described methods [57]. Donors provided informed consent for biopsy. Permission was obtained for specimens taken from organ donors. Primary keratinocytes were cultivated with a feeder layer in a culture medium. The feeder layer was composed of fibroblasts of the cell line 3T3 J2, obtained from embryonic mice tissue, needed to initiate keratinocyte colony formation [57]. The cells were seeded with DMEM and 10 % Newborn Serum (NB). After that they were irradiated (50 Gy) and seeded again in a F75 (approximately 2 million cells for the whole surface). Pre-confluent or newly confluent first-passage primary human keratinocytes were trypsinized and seeded at a density of 1×10^5 cells per 100-mm dish onto the feeder layer. After 3 days of culture, keratinocytes were transduced by incubation with a recombinant EGFP-expressing LZR-based lentivirus generated by transient transfection

in 293T cells, as described [58]. After two infections, the cells were given fresh medium and allowed to reach 80-90 % confluence. Keratinocytes were then trypsin detached, analyzed for EGFP expression and sorted.

All cellular cultures were always manipulated inside biosecurity cabins (Telstar, Bio IIA/G) and cryopreserved when needed at -83 ºC in a freezer (Unicryo DW-86L286) using freezing medium Dimethyl Sulfoxide 10 % (DMSO, Sigma Aldrich) in FBS.

3.2.2. Plasma-based Artificial Skin Construction

The basis of the skin models is to generate a functional dermal component that interacts dynamically with the keratinocytes during *in vitro* maturation as well as *in vivo* after graft transplantation. To do so, fibrin gels are created from fresh frozen human plasma, taking advantage of the human endogenous fibrinogen coagulation process aided by calcium cations (Ca++).

The fresh plasma was obtained by the primary separation of blood of donors from the blood bank of Asturias (Centro Comunitario de Transfusiones del Principado de Asturias), following the rules and recommendations of American Association of Blood Banks [59]. Plasma-based dermal grafts were prepared in 6-well plates (Costar, Corning). For each fibrin gel 3 ml of final product were prepared. First, 4000 cultured fibroblasts were added (1000 per cm^2) to 1.5 ml of a saline solution (NaCl). Cells were counted in a Neubauer chamber, and their viability was assessed with Trypan Blue solution [60]. Then, 24 µl of tranexamic acid (Amchafibrin, Fides Ecofarm, Barcelona, Spain) were added to inhibit fibrinolytic activity from the fibroblasts. Finally, 1.75 ml of fresh human plasma (2.44 mg/ml of fibrinogen) were added, along with a $CaCl_2$ solution to induce fibrin coagulation. The mixture was placed on the plates. Solidification was complete after 2 hours of incubation at 37 ºC, and culture medium was added. One day after 1.5 million of purified $EGFP^+$ healthy, RDEB were seeded on the corresponding fibrin matrices to form the epidermal layer of the artificial skin. The complex was cultured until keratinocytes confluence was reached.

3.2.3. *In vivo* Regeneration of Artificial Human Skin

Genetically engineered skin constructs were manually detached from the plate and placed orthotopically on the backs of immunocompetent mice. Four mice were grafted (two healthy, two with RDEB). Briefly, mice were aseptically cleansed. Full-thickness 12 mm circular wounds were then created on the dorsum of mice to match skin equivalents as seen in Figure 23 A. Mouse skin removed to generate the wound was devitalized by three repeated cycles of freezing and thawing and used as a biological bandage, fixed

with sutures, and covered to protect and hold the skin substitute in place during the take process (Figure 23 B-H). Dead mouse skin was expelled, generally within 15 days of grafting, and regenerated human skin became visible Figure 23 I, J. Grafting was performed under sterile conditions, using 6-week-old female NUDE mice purchased from the Janvier Laboratory and housed under pathogen-free conditions for the duration of the experiment at the *Centro de Investigaciones Energéticas Medioambientales y Tecnológicas (CIEMAT)*, Laboratory Animals Facility. Animals were housed in individually ventilated type II cages, with 25 air changes per hour and g-irradiated (10-kGy) soft wood pellets as bedding.

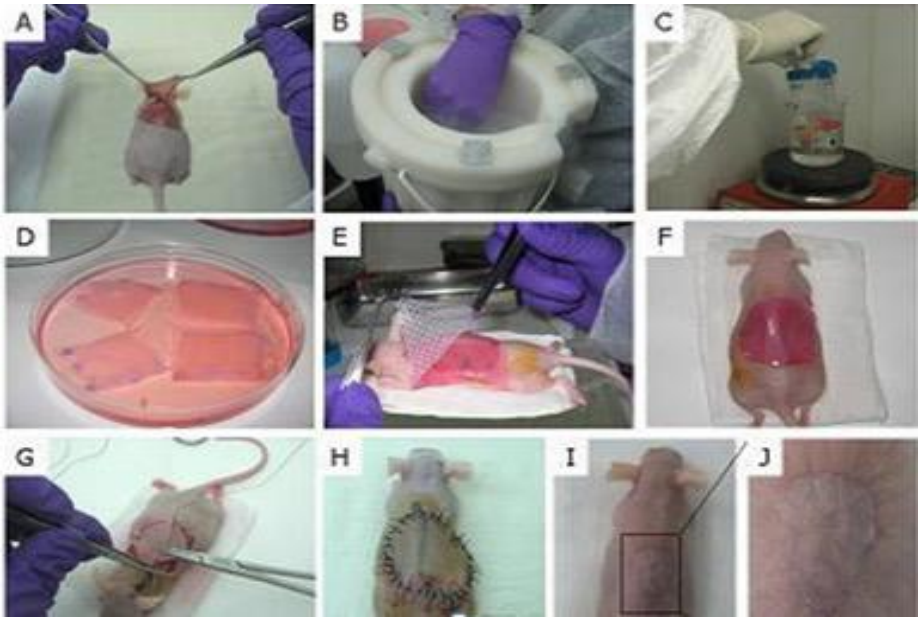

Figure 23: *Transplant procedure of human skin equivalents. A) Mouse skin removal. B), C) Freezing and thawing (respectively) cycles for mouse skin devitalization. D) Skin equivalents prepared for transplant. E), F) Implantation. G), H) Stitching of previously devitalized skin on top of the implanted skin to make a biodegradable and biocompatible bandage. I), J) Human skin regeneration in mice.* [61]

The transplant was analyzed under fluorescent light microscopy to observe its maturation stage. After 8 weeks, it was successfully integrated, and mice could be taken to perform the *in vivo* device experiment.

3.3. *In Vivo* Testing: Blister by Suction

Mice were observed under fluorescence to determine the section of human skin that was present. Green fluorescence was readily visualized in the intact xenograft *in vivo* (Figure 24), using a fluorescence stereomicroscope under blue light (Olympus America, Melville, NY). Before applying any suction, the incandescent light bulb was set on top of the area

to be examined, approximately 2 cm away, for 2 minutes. The heat received at such distance in the skin was calculated approximately to be 35 ± 5 ºC. After that, the bulb was kept on for the entire duration of the experiments to maintain the heat.

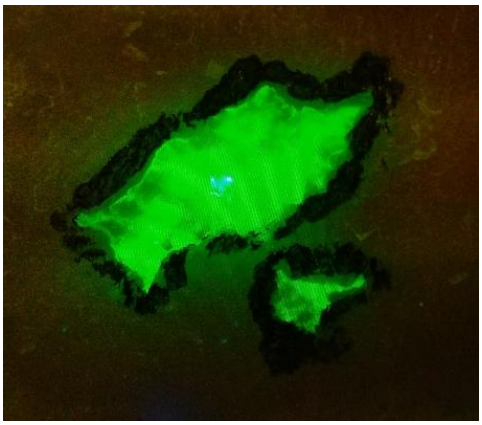

Figure 24: *Green fluorescence in xenograft in vivo.*

Figure shows examples of how the suction device was employed in the different experiments. An initial trial was performed to obtain an idea of how much time and pressure was needed to generate the blister. With a big outlet (9 mm), that span the small section of human tissue as well as that of the animal, suction was applied to a delimited area of the skin as seen in Figure 25 b. After that, the outlet was changed to a smaller cross section (3 mm) to increase pressure force on the skin, considering pressure as $P = \frac{F}{S}$.

Three experiments were completed on another mouse with regenerated RDEB human skin. In this model the human skin surface *taken* by the mouse span a big area, which made it possible to do three separate tests. The previous assessment was taken into consideration to choose the conditions applied. First, the device was set to maximum pressure for 7 minutes. For the second and third tests, the pressure was lowered to 80-85 kPa and applied during 7 and 5 minutes respectively. Moreover, two control models were tested for 5 minutes at 65-70 kPa and 80-85 kPa. Examples of the process can be seen in Figure 25 c-f, including the control model.

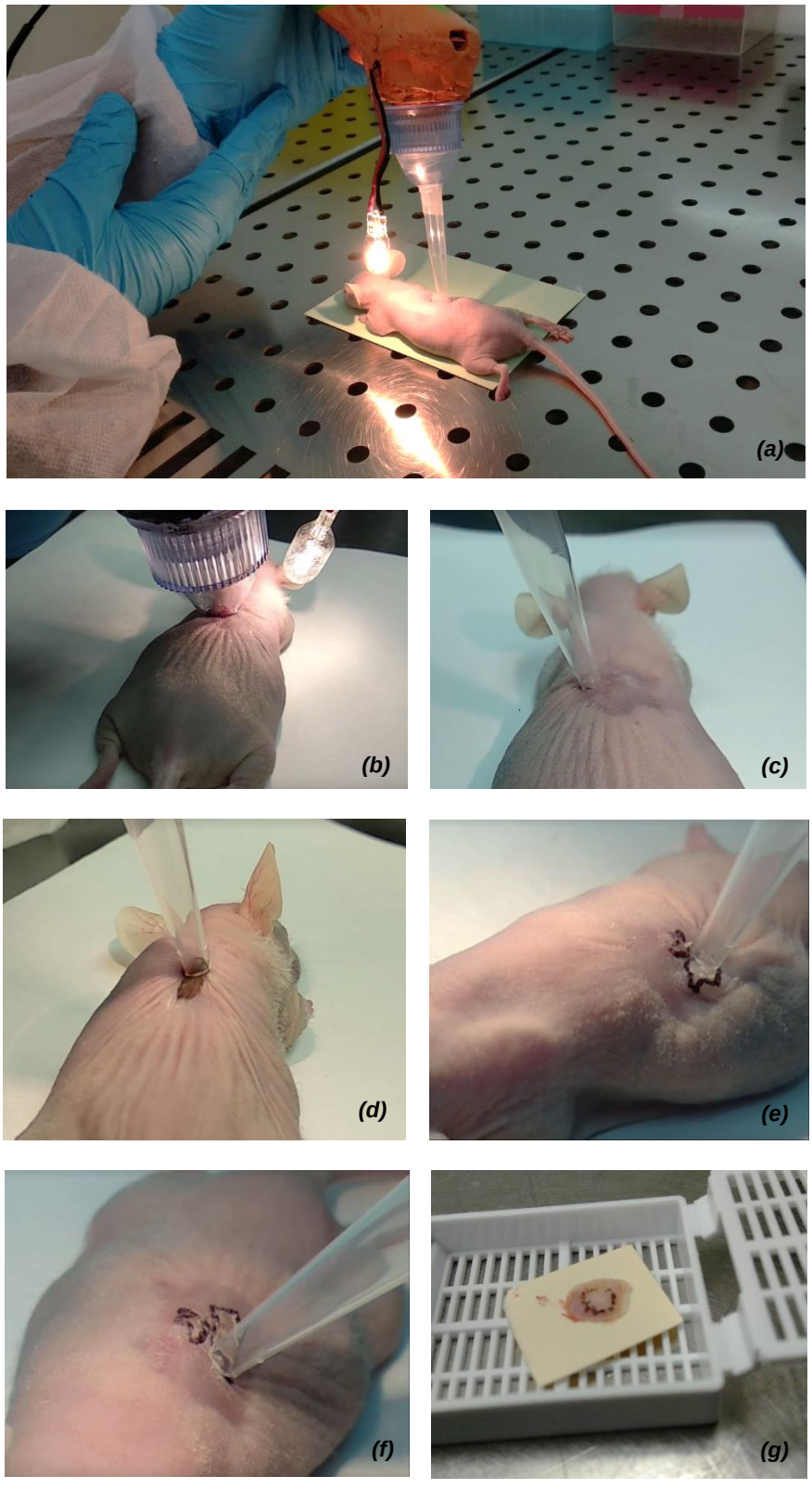

***Figure 25**: In vivo experiments on the regenerated human plasma-based skin grafts. (a) Overview of the device being applied to the mice model using the small outlet (3mm). (b) Initial assessment with 9 mm outlet. (c) Initial assessment with the smaller 3 mm outlet at maximum pressure for minutes. (d) Test on control model for the same conditions (C1). (e), (f) Second and third experiments (E2, E3), with the 3 mm outlet. (g) Biopsy of the human skin graft (delimited in black) with a margin of approximately 2 mm of surrounding mouse skin.*

To complement this work, the device was tested on a mouse with a skin graft corrected to produce C7. This was provided by a laboratory group within CIEMAT, which had produced genetically edited human skin mice models using CRISPR/Cas9 complex. A mutation in exon 80 of COL7A1 gene (c.6527insC) was the target for the gene editing approach. CRISPR/Cas9 pairs flanking exon 80 were delivered to primary patient keratinocytes by electroporation. Keratinocytes used were obtained from the same patient that provided the cells for this present work. Gene correction was done by NJHR. Skin equivalents were generated with polyclonal keratinocyte cultures in which COL7A1 reading frame had been restored and C7 was being expressed. Normal human skin was developed upon transplant onto immunodeficient mice. These grafts showed C7 deposition at the basement membrane zone, formation of anchoring fibrils and structural integrity when analyzed ten weeks after grafting. This proved that epidermal stem cells, able to sustain long-term skin regeneration, had been successfully corrected.

The last conditions tested (5 minutes at 80-85 kPa) were applied to half of the grafted human skin, the other half taken as control sample.

The experiments are summarized in Table 3.

Table 3: *Summary of suction skin splits, combinations of skin type, time and pressure applied.*

	Skin type	Time (min)	Negative pressure (kPa)
Control 1 (C1)	Healthy	5	65-70
Control 2 (C2)	Healthy	5	80-85
Experiment 1 (E1)	RDEB	7	65-70
Experiment 2 (E2)	RDEB	7	80-85
Experiment 3 (E3)	RDEB	5	80-85

The regenerated human skin grafts were excised after 5 minutes (to allow the blister to settle) along with approximately 2 mm of surrounding mouse skin (Figure 25 g). To maintain the tissue in a reliable state compared to the living one, the excised samples were placed in 10% buffered formalin for paraffin embedding for further analysis.

3.4. Analysis of Regenerated Artificial Human Skin Split by Suction

The tissue biopsies taken were fixed in 10% formalin. For paraffin embedding, the tissue was treated with a series of graded ethanol solutions (VWR Chemicals Prolabo) to dehydrate it. Moreover, to remove the still non-miscible (in paraffin) alcohol, remaining

fat, and increase transparency, the samples were introduced in xylene (Scharlab S.L.). Tissues were carefully placed in melted wax at 58 ºC for 15 minutes and solidified by freezing. A microtome (Leica RM2255) was used for cutting the sample into 5 µm slices. The slices were rapidly set in water at 40 ºC to smooth them out and placed in glass slides (Super Frost Ultra Plus, Thermo Scientific). Before histological and immunohistochemical studies, the samples were deparaffinated with sequenced reduced ethanol concentrations and xylene.

3.4.1. Histological Analysis: Hematoxylin and Eosin Studies

Samples were stained following the standard procedure. First, the tissue was rehydrated in three consecutive alcohol solutions (100 %, 95 % and 70 %). Then, samples were introduced in hematoxylin stain for 5 minutes and washed to remove the excess with HCl 1 %. After that, the slides were placed in Bluing reagent for 1 minute. Then, they were washed in running tap water and rinsed in 95 % alcohol before they were counterstained with eosin for 5 minutes. After rinsing the excess stain, samples were dehydrated in consecutive alcohol solutions (70 %, 95 % and 100 %) and cleared in xylene. Finally, the samples were mounted and visualized under the microscope to determine if blisters were present. Six slides of each tissue were selected, where most prominent blister was seen, to perform the corresponding immunohistochemical studies.

3.4.2. Histological Analysis: Immunohistochemistry Studies

In experimental grafting protocols, formalin or ethanol fixed sections were stained using specific antibodies against human collagen VII (Col7 LH 7.2, provided by Dr. Nyström, University of Freiburg, Germany), anti-human cytokeratin 10 (monoclonal AE2, ICN Biomedicals, Cleveland, OH), anti-human cytokeratin 14 (clone LL001 Santa Cruz, USA) and anti-human vimentin (V9, BioGenex, San Ramon, CA). The last antibody was applied to ensure the presence of fibroblast in the dermis.

An immunoperoxidase analysis was done to detect collagen VII in the selected samples. Proteinase k (DAKO Agilent S-3004) was dissolved in Tris-HCl 50 mM for antigen retrieval during 10 minutes at room temperature. After washing with PBS 1X, the tissue samples were incubated for 30 minutes with a solution of 0.1 % Triton (Merck) and 3 % H_2O_2 in PBS to inactivate endogenous peroxidase activity. Then, they were washed again, and the unspecific binding was blocked by incubating in 3 % Bovine Serum Albumin (BSA, Merck) in PBS for 30 minutes at room temperature. The primary antibody Col7 was left to react overnight at 4 ºC. The next day, the secondary antibody was incubated for 45 minutes. Then, the secondary antibody detection was done with the

avidin-biotin complex (ABC, Vesctastain) kit, which was placed on the samples and left in the dark for 40 minutes. Finally, after removing excess with PBS, the tissue samples were developed with DAB (3, 3 -diaminobenzidine) HRP substrate (Vector). DAB is oxidized when reacting to hydrogen peroxide, which is present in the peroxidase enzyme conjugated with the antibody, thus producing a brown precipitate. The intensity of the color was controlled under optical microscope and stopped by non-distilled water when appropriate.

For vimentin, cytokeratin 10 and cytokeratin 14 immunohistochemical analyses, the antigen retrieval was heat mediated. The samples were placed in a 2 % citric acid and 8 % sodium citrate solution and heated at 300 W up to boiling of reagent. The endogenous peroxidase was blocked then with a 0.3 % H_2O_2 in methanol solution for 10 minutes. The sample was blocked with 3 % BSA/PBS for 45 minutes, and the respective primary antibodies were placed overnight on each tissue sample. The following steps were the same as described for the collagen VII assay.

All samples were counterstained with hematoxylin to guarantee nuclei observation, dehydrated and cleared as previously explained, and mounted with the Shandon Xylene Substitute Mountant machine (Thermo Scientific).

4. RESULTS

4.1. Suction Device

When the device was correctly assembled and programmed to perform the desired functions, it was examined to verify the basics. The end product can be seen in Figure 26. To set it up, only three steps must be followed: plug the charger to a regular wall socket, connect it to the mini USB inlet at the bottom, and insert the outlet chamber.

Figure 26: *Finalized device. Included in the picture are the OLED screen, incandescent light bulb, outlet chamber and mini USB charger cable.*

To assess the behavior of certain components, a computer program was used, Telemetry Viewer. By connecting the microcontroller to the computer, it was possible to obtain real time measurements of the desired signals sent to and from the digital or analog pins. First, it was important to confirm that potentiometer changes modified the PWM signal accordingly. In Figure 27 both signals are plotted at the same time, between 0 and 5 V. It can be seen that the changes in potentiometer values correspond to changes in PWM (according to Equation 1), which then modify the power of the motor.

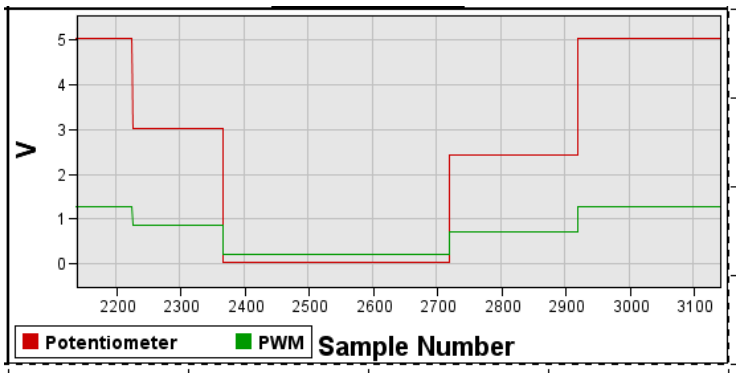

Figure 27: *Potentiometer and PWM voltage signals sampled through time.*

Having confirmed that, the functioning of the pressure sensor is assessed. The scaled graph from Figure 28 shows the evolution of sensor voltage throughout 1000 samples at maximum pressure (lower than 65-70 kPa, as it is supplied by the 5 V provided by the USB computer connection and pressure does not reach the maximum measurable by the sensor). It is clear that the pressure signal fluctuates over time, but the deviations should be neglected as the scale is small, 0.01 V. The change observed corresponds to pressing the sensor outlet on the skin, which lowers the pressure as the surface is covered and air is not flowing freely.

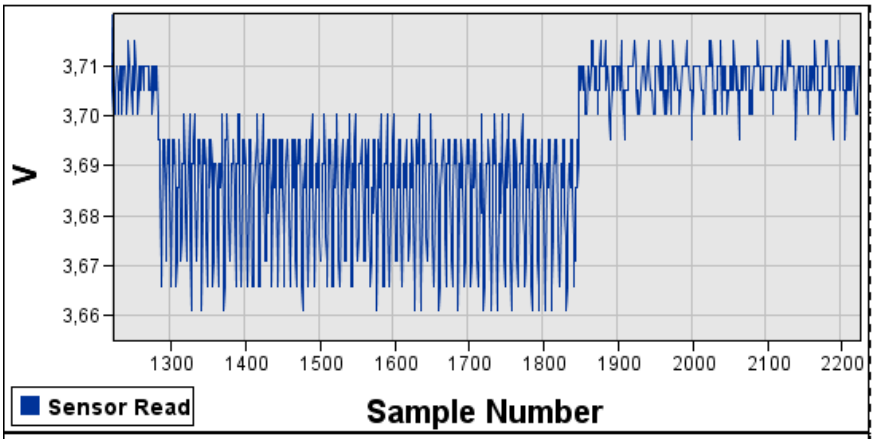

Figure 28: *Voltage signal from the pressure sensor.*

4.2. Suction Split Skin Analysis

The skin was left for 5 minutes after application of vacuum to allow blister settlement. The pictures in Figure 29 were taken at that moment, before obtaining the biopsies. They show a macroscopic overview of the skin grafts after applying suction. The black lines limit the area of human skin within the mouse's back.

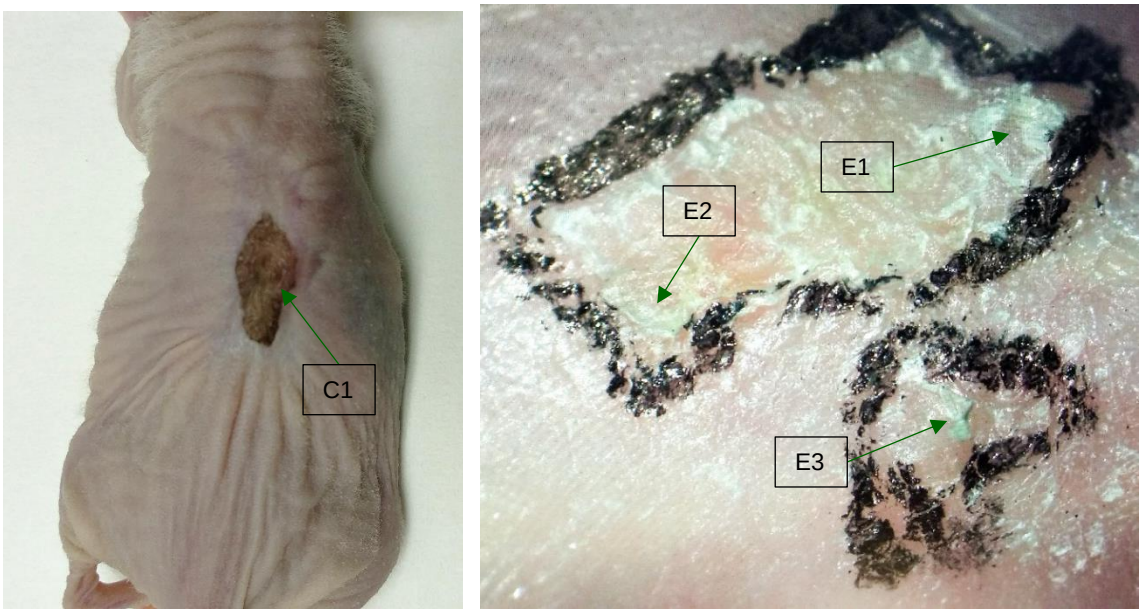

Figure 29: *Macroscopic view of suction-induced blisters before excision. C1: 5 min 65-70 kPa. E1: 7 min 65-70 kPa. E32: 7 min 80-85 kPa. E3: 5 min 80-85 kPa.*

In the first image of Figure 29 the first control model is shown, after suction. In the first experiment (E1), the induced wound appears to be smaller, as does the third one (E3). In the case of experiment 2 (E2), the blister generated is in a circular shape, being approximately the size of the device as well. For E3, the blister area appears to be elevated upon first sight, in the conventional way a regular blister would be in healthy skin (from a small burnt for example).

The stained samples were observed under light microscopy and pictures were taken on relevant sections of each.

4.2.1. Microscopic Confirmation: Hematoxylin and Eosin (H&E) Stain and Immunohistochemical Studies

Upon first observation of the samples, the regions of interest within the different experiments were selected for further histological analysis. H&E stain was decisive as it provides a general view of the tissue structure and components. In this step, the

consequences of each experiments were determined, and the slides of most importance were selected for the subsequent analyses.

In Figure 30 a and b, two images taken from the control samples are shown. The first one (a), is of a section where suction was applied (C1, 65-70 kPa for 5 minutes). The second, (b), is taken from an area where no forces were induced. No damage is found in any of the images, which implies that blistering only occurs in diseased skin (with the times tested).

For the first experiment (E1), with maximum pressure (60-65 kPa) for 7 minutes, the dermis appears to be torn and the skin extended upwards, as seen in Figure 30 c, d. The dermoepidermal junction appears ripped as well (asterisks in Figure 30 d), but more extensive holes are seen in the dermis (circle in Figure 30 d). Figure 30 e shows the blister generated in E2. It is considerably big, but dermal breakage can be still observed. The third experiment produced a definite blister with minimal dermal disruption (Figure 30 f).

As well as the H&E stain, the analysis of vimentin allows for distinguishing the structural integrity of the dermis. In Figure 31, control (a) and RDEB (b, c, d) samples are shown to compare dermal integrity. Healthy skin conserves proper structure of both epidermal and dermal components, while diseased skin in E1 (Figure 31 b) has completely lost it after the experiment. In (c) the results from E2 can be observed. Blister appears with some minor dermal damage. Finally, (d) is an image taken from E3, where the dermal component is almost intact, and no lesions are observed except for the blister at the DEJ.

To verify that the formation of blisters is caused by absence of collagen VII (C7) in the RDEB skin equivalents, immunohistochemistry studies with antibody against human C7 were done and control and EB samples were compared (Figure 32). C7 appears in a brown color along the dermal-epidermal junction, while cell's nuclei were counterstained in blue for better visualization. The blister generated in E3 can be seen in Figure 32 b, and it is corroborated that C7 was not present in the tissue sample due to the RDEB condition of the cells.

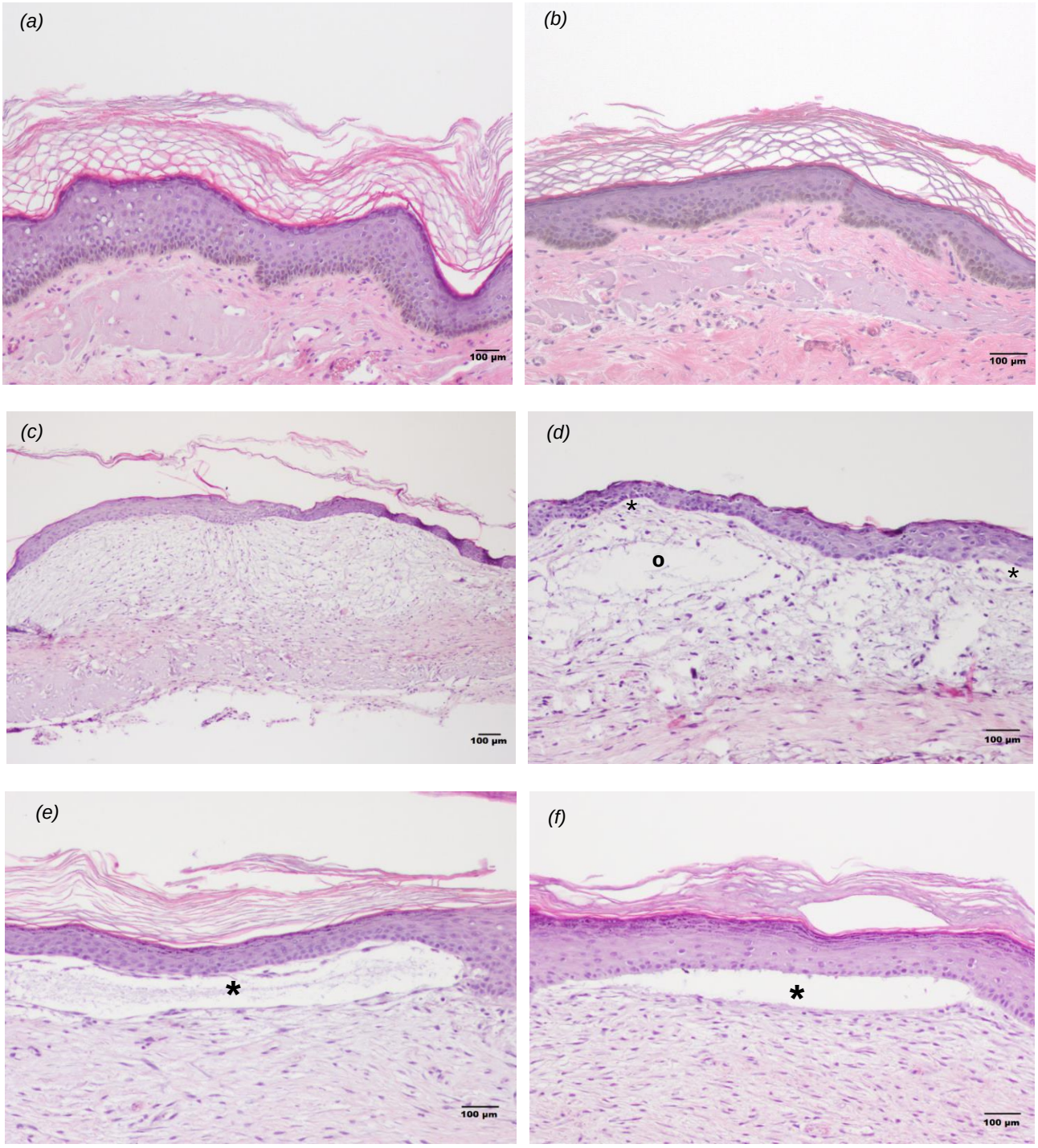

Figure 30: *Hematoxylin and Eosin stained images. Blisters on the DEJ are pointed out by asterisks and those on the dermis are designed by circles. (a) is an image from C1 (10X). (b) is an image of a healthy sample with no pressure applied to it (10X). (c) and (d) correspond to images taken of the samples of E1, with 4X and 10X lenses, respectively. The pressure and time was excessive, and the dermis torn all over, with intradermal blistering. In (d), the blister formed in E2 is shown at a resolution of 10X. (e) presents a 10X image of the blister formed in E3.*

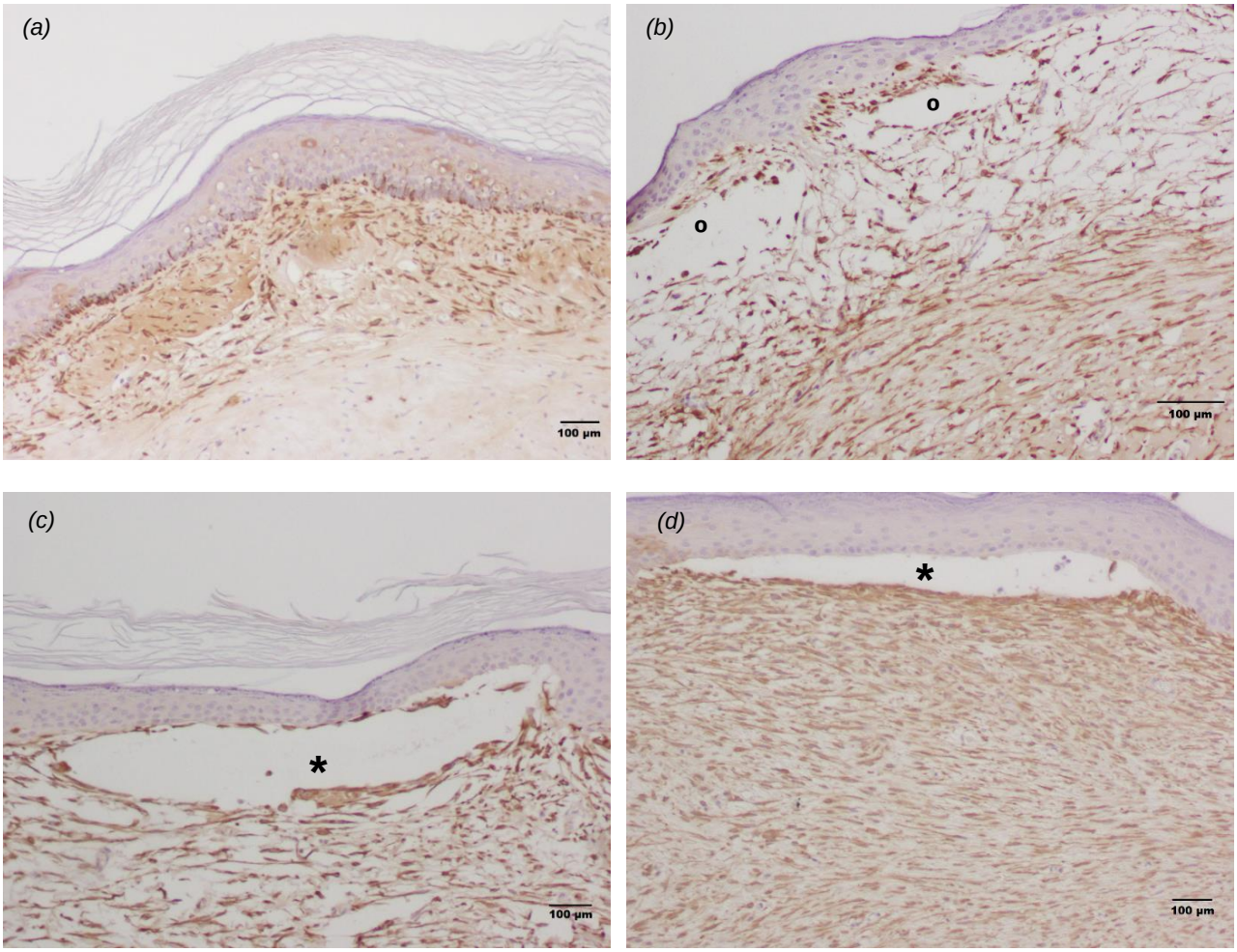

Figure 31: *Vimentin immunostaining. Blisters on the DEJ are pointed out by asterisks and those on the dermis are designed by circles. (a) corresponds to the second control sample (10X), where tissue integrity is intact with healthy collagen fibers. (b) is an image of E1 (10X), where the dermis is structurally compromised, and intradermal blisters are seen. (c) image from E2's big blister with certain dermal damage and small intradermal blisters (10X). (d) blister generated in E3, no intradermal blistering and minimal extension of the dermis (10X).*

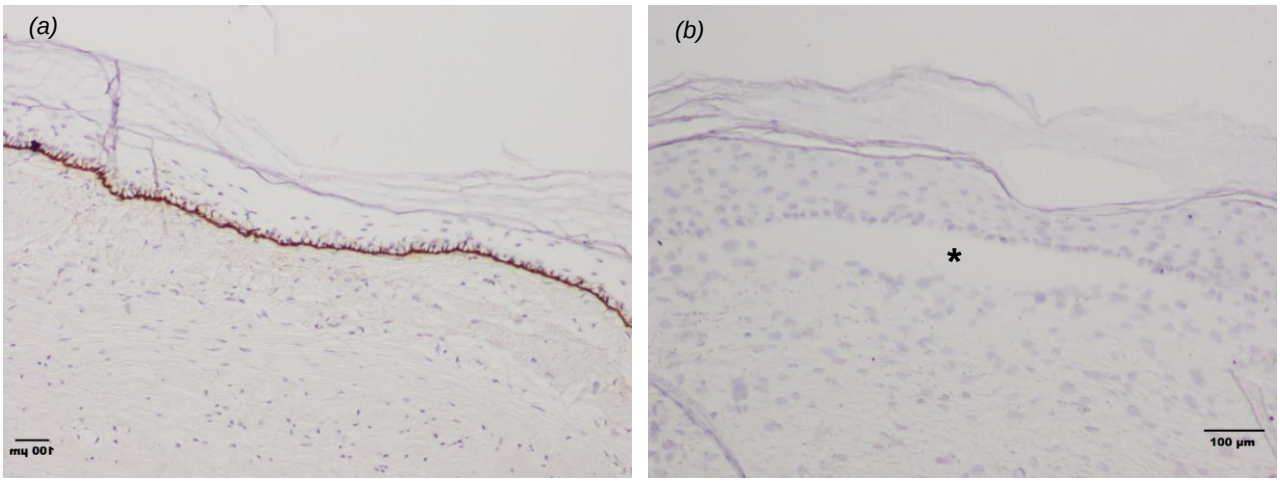

Figure 32: *Collagen VII immunostaining. Blisters are pointed out by asterisks. (a) shows the healthy control sample in 10X resolution and (b) shows the blister formed in experiment 3 without C7 presence (10X).*

Stains against specific markers of the epidermis were performed to determine how well the skin equivalents were differentiated and developed, and the level of rupture during blistering in E3. In all samples (control and RDEB). The two proteins studied were situated in the appropriate locations, as seen in **Figure 33**. Cytokeratin 10 (K10) can be observed in the suprabasal layers, up to the stratum corneum; while cytokeratin 14 (K14) is only seen in the basal keratinocyte layer. In addition, the images verify that blisters were formed at the dermal-epidermal interface, with no keratin appearing below the blister (**Figure 33** c, d).

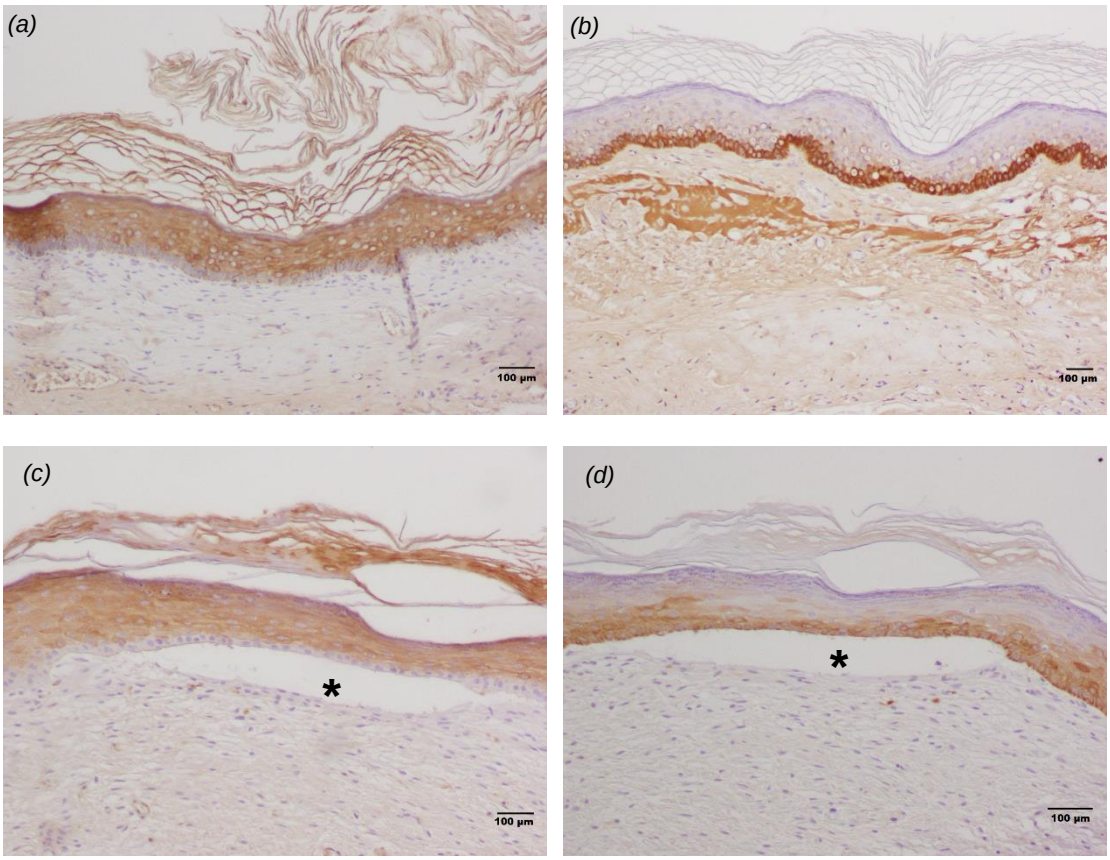

Figure 33: *Cytokeratin 10 and 14 immunostaining. Blisters are pointed out by asterisks. On the top row, the control samples are shown, and in the bottom, E3 blister. All pictures were taken at a 10X resolution, stained for K10 and K14 and counterstained in blue for nuclei. (a) and (c) are taken from the K10 immune assay. Colored areas correspond to this protein's location in the suprabasal epidermal layers. (b) and (d) correspond to the K14 stain. Hence, color is seen in the basal kerainocytes. (b) appears to be stained in the dermal layer as well, due to too much time of exposure to developing substance.*

4.2.2. Gene Edited Human RDEB Skin

The suction device was tested on an animal model provided by a research group within CIEMAT where by gene editing, the same mutated skin used in our studies were corrected for C7. A negative pressure of 80-85 kPa was applied to the skin for 5 minutes, to corroborate that the gene editing procedure was successful. Figure 34 shows the H&E stained samples, one where pressure was applied (b) and a control one (a). Figure 35 shows images of these two samples as well after an immunohistochemical assay for collagen VII. It is clear from both sets of images that the gene editing process was effective. The tissue structure was conserved before and after suction, and C7 is visible correctly in the DEJ as shown in Figure 35. No dermal damage or blisters were found.

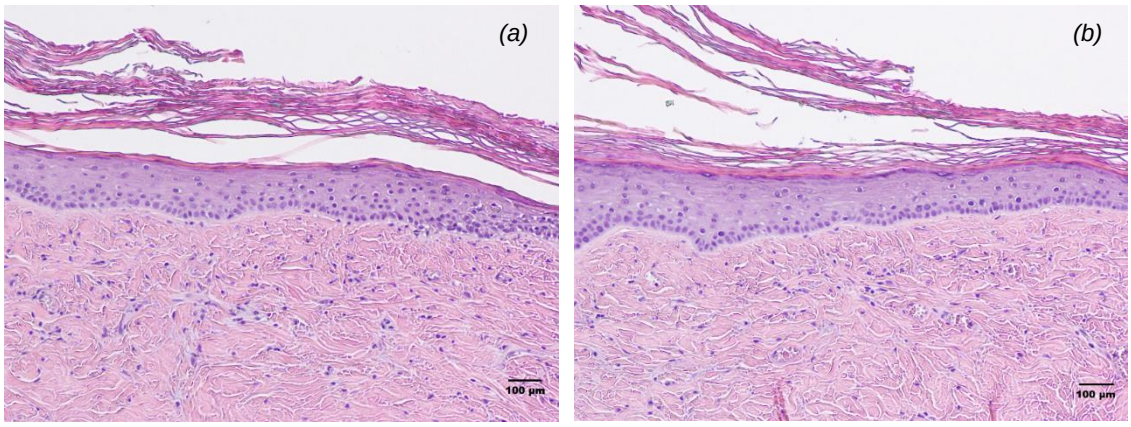

Figure 34: *Hematoxylin and Eosin stained images of COL7A1 corrected skin equivalent. (a) is taken from the control sample (10X), where no pressure was applied, and (b) is from the area where 80-85 kPa were applied for 5 minutes (10X).*

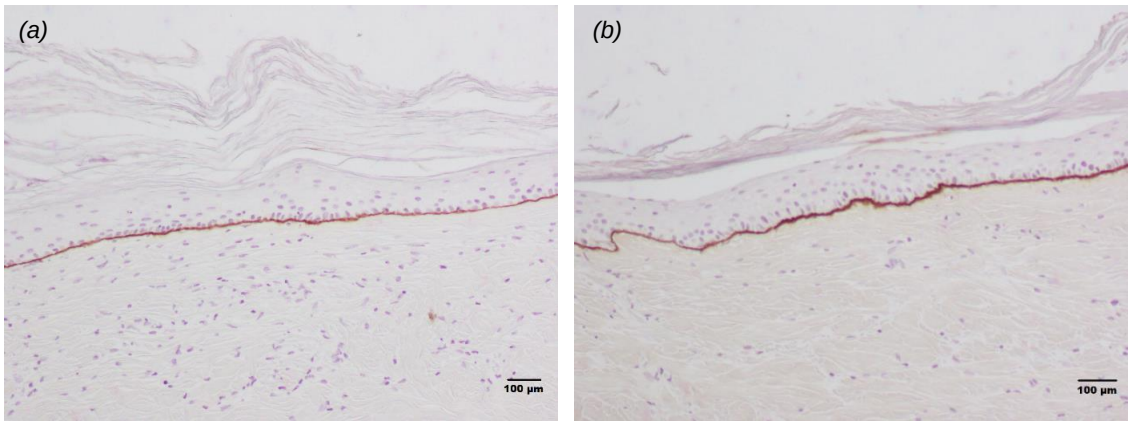

Figure 35: *Collagen VII immunostaining of samples of COL7A1 corrected skin equivalent. (a) is taken from the control sample (10X), where no pressure was applied, and (b) is from the area where 80-85 kPa were applied for 5 minutes (10X).*

5. DISCUSSION

In the present study, the generation of blister wounds in Recessive Dystrophic Epidermolysis Bullosa was studied. It has been established [48] that blistering time is an indicator of dermoepidermal adherence, which leads to diagnosis of skin disorders such as Epidermolysis bullosa. Previous reports have been found where suction has been used as a method for generating blisters for diagnostic purposes in EB and other genodermatoses [44], [45], [49]-[51]. Based on the relationship between blistering time and DEJ adherence, which can be correlated to a specific skin disorder, a standardized methodology must be generated and applied so that a unified diagnostic criterion exists in such cases. This is extremely important in rare diseases, which often have few treatment options available, and early diagnosis can speed the access to it. In addition, the more patients are identified to have such diseases, the more research advances are made in their field. This work focused on determining the optimal blistering time for RDEB, a severe type of the rare disease Epidermolysis bullosa.

To do so, a suction device was developed to fit the desired characteristics. The key parameters to be considered were negative pressure and time, with the temperature of the tissue influencing the events. To have distinct and real-time data of these variables, a sensor was introduced, as well as a small screen to see the values without having the device continuously connected to a computer. This would have defeated one of the main objectives of the project, having a manageable tool for comfortable use in future every day clinical diagnostics. A timer was established in the microcontroller to determine how long the suction was applied for. A core component is the Arduino-compatible board. It proved to be a simple and easy to use microcontroller, providing every function that was needed with option for personalization due to its open-access software [30]. Basic electronic components such as resistors and a diode were introduced along the process to avoid excessive current and damage. After trying out the finalized product, it was clear that the choices were correctly made. The device is easy to set up, only needing to insert the outlet chamber, plug the charger into the micro USB connector, and check if the screen is correctly connected. All elements are shown in Figure 26. It was important to achieve this, as the precedents for this project are bulky, multi-piece devices uncomfortable for the patients and clinicians [50], [52].

RDEB human skin equivalent mice models were generated for testing the device and determining the correct parameters through histological analysis. Healthy models were created as well for reference purposes. The method employed was described in previous

works [29]. A dermal component was generated by employing a mechanism present in wound healing, fibrin clotting. A scaffold for fibroblasts to be embedded on was created that way, which also served as support for the epidermal component (keratinocytes). Amongst the advantages of this bioengineering method, the possibility of building a completely autologous skin graft is one of the most important. The three main components can be obtained from the patient. In cases such as EB, where the cells are at fault for the disease, gene editing methods could be introduced to complement and complete the therapy [18], [22], [24].

Skin regeneration on the animal models was done by qualified scientists, and after two months they were completely differentiated and available for testing. In healthy skin equivalents, tissue architecture was developed properly, with accurate dermal structure and epidermal differentiation (Figure 30 a, b). For the RDEB models, tissue was properly formed as well, without collagen VII due to the condition of the cells within the tissue, as seen in Figure 32 b. For both types, the histology images give a good impression of the constitution of the skin grafts. The dermis had the proper configuration as evidenced in the vimentin examination (Figure 31 a, control sample). In all cases (healthy and diseased) the epidermal component presented no damage in any of its layers, as evidenced in the cytokeratin immune assays in **Figure 33**. Cytokeratin 10 and 14 were observed in the corresponding epidermal layers (suprabasal and basal keratinocytes, respectively). None of these proteins must be compromised in RDEB grafts, as it only affects collagen VII in the DEJ [55].

Regarding the blister generation on the actual human skin models, the analysis of the results provided a combination of time and pressure to create a proper blister. First, it is necessary to define what a «proper blister» is. Taking into account that this work is dealing with RDEB, a good resulting blister would be one that separates the dermal and epidermal components, without any of them ending up torn or damaged.

In experiment 1 (E1), the maximum pressure was applied (65-70 kPa) for 7 minutes. By exerting the same force during a longer and continuous time period, the errors found in the previous experiment could have been corrected. In reality, when analyzing the histology images, it is clear that such pressure was excessive. The tissue extends upwards into a dome-like shape. The dermis looks separated, with holes in between fibers and cells, and even intraepidermal blistering (Figure 30 c, d). This is also evident in the vimentin immunostaining images of Figure 31 b compared to the correct structure in the healthy model (a).

All in all, a high negative pressure of 65-70 kPa (the maximum capacity of our device) was proven to be excessive for the generation of a proper blister in RDEB models. The skin is fragile, and even though collagen VII is not present throughout the dermis, this experiment proves that its anchoring function plays a role in dermal integrity. However, for other less severe subtypes or different EB types (where the protein at fault plays another role, see Annex) it may be appropriate to use such magnitude.

Experiment 2 introduced, for 7 minutes, 80-85 kPa of negative pressure. Applying a smaller force was thought to increase the chances of not ripping the dermis. Righteously so, when the histology samples were analyzed, the dermis looked as if it had suffered substantially less trauma. A blister can be distinguished at the dermal-epidermal junction (Figure 30 e), but, when analyzed closely, it is evident that it is part of the dermis, as some fibroblasts are present on the blister roof. In addition, other minor dermal blisters can be observed below, as consequence of the rupturing and destructuralization that the suction induced (as seen in vimentin study Figure 31 c).

Finally, in experiment 3 the medium vacuum (80-85 kPa) was applied for 5 minutes. After analyzing the histology samples, it was clear these were the best conditions. In Figure 30 f, the blister generated appears to be a clear separation of the epidermis from the dermis, as evidenced in the smooth joining at the two flanking sides. No fibroblasts appear still joined to the epidermis. The dermis is not torn in comparison with the other samples. Compared to the healthy subjects, the extracellular matrix looks slightly separated, if not almost intact, as it can be seen in the vimentin assay's images from Figure 31 d. Consequently, it was concluded that the optimal conditions tested out in this work were those of Experiment 3. The pressure applied was enough to generate a delimited blister on the skin graft, but not too much so that damage was done. In the same manner, it was applied for a sufficient amount of time to obtain the proper results.

Temperature played an important role in blister generation. As mentioned before, an increase in this parameter in the specific area stimulates the molecular processes that occur within it [48]. Therefore, the separation of epidermis and dermis at is produced by rupture of DEJ, benefited by heat. While suctioning of the skin provokes splitting by mechanical forces, temperature aids in formation of the desired blister. In a recent study assessing the potential of mesenchymal stem cell therapy in RDEB child patients, suction blisters were introduced to evaluate DEJ integrity before and after treatment [51]. A vacuum device was employed, set to deliver 12-15 mmHg (1.5-2 kPa) with heat being directly and constantly applied to the skin. Blistering times in patients were about 10 minutes. Even though temperature values are not specified in the report, it can be extracted that this parameter influences the outcome significantly. This is indicated by

the fact that small blistering times, similar to those resulted in this work, are obtained with minimal pressure. Consequently, the proper temperature value, delivered in a non-changing environment (the suction chamber) can substitute a higher suction force in generating blister for RDEB.

The pressure ranges selected for all the experiments are consistent with the most recent study analyzed, from Stanford University researchers [52]. Similar blistering times were obtained, under a slightly lower negative pressure (5.7 min at approximately 91 kPa). The results are comparable to those obtained in this work, where a higher suction force (80-85 kPa) generated a blister in 5 minutes.

In said research project, heat was delivered to the skin in a controlled way (heat ring at 37 ºC). In the present work, temperature was not constant throughout the experiment, first applying it alone to warm up the skin, and then outside of the chamber during the suctioning process. Obtaining similar results with different temperature conditions suggests that, with high suction, temperature plays a secondary role in blister generation. Nevertheless, heat delivery should be improved for reproducibility of experiments in future work.

The fact that at the same time, two completely independent research projects, with dissimilar instruments, obtained almost the same result proves up to a certain level that they are accurate. Furthermore, it is an indication of the significance of the research and how important it is to expand it.

6. CONCLUSIONS

- As dermal-epidermal adherence is a decisive parameter on EB diagnosis, we have generated a precise device to substitute the current RDEB diagnostic method by a more precise, reproducible and reliable one.
- An easy to use device represents a less invasive method of diagnosis that betters the life of patients that may have severe conditions such as RDEB.
- The ideal combination of negative pressure and time to produce a proper blister in RDEB skin (mutation c.6527insC) is 80-85 kPa for 5 minutes.
- The device can be implemented in different research projects, for example, to prove DEJ integrity in genetically corrected mice models.

7. LIMITATIONS AND FUTURE WORK

The objectives of this work were positively achieved and have been presented throughout this thesis. Nevertheless, some limitations and improvements can and must be done to both the device and testing methodology.

First and foremost, the device must be tested in patients, to eliminate the limitations that an animal model presents. Even though the human skin equivalents do achieve their purpose, tissue structures are missing from these models, such as other cell types, hair follicles, or sensory receptors. Disease characteristics may not be fully replicated as other factors influence DEJ integrity.

As the clinical level cannot be easily reached, other methods must be applied to improve the work that has been done. Skin models from different patients must be generated, as genotypes are different within the same condition, and other optimal suction and time combinations may be found for RDEB. Healthy samples' blistering times should be measured in further studies. Moreover, the device should be tested for other types and subtypes of EB. Different mutations give rise to the phenotypical heterogeneity of this disorder, with less severe conditions that will result in higher blistering times.

Regarding the device, there are certain aspects that must be improved. It was generated as a first draft, to test the hypothesis. The objective was to create the tool keeping in mind that it would be bettered in future works. First, the heating mechanism should be further developed, by including a temperature sensor to have this data real-time on the screen, along with the pressure and time. Additionally, the heating mechanism can be substituted by a specialized heating component. This could be introduced inside the suction chamber that is in contact with the skin. In that way, the heat is delivered directly to the selected area by convection while applying the negative pressure, and the effect of temperature in blister generation would be more effective. For future development of the device, the incandescent light bulb should be changed, as there is a risk of it breaking and damaging the patient (in this case, the animal model).

Finally, the accuracy of the current pressure sensor should be assessed. As seen in Figure 28: Voltage signal from the pressure sensor., the readings from this component vary in time. A mean of the values registered during blistering time could be obtained and delivered in the screen at the end.

8. REGULATORY FRAMEWORK AND SOCIOECONOMIC IMPACT

8.1. Regulatory Framework

The device developed in this work falls into the category of Class IIa active medical devices intended to be used transiently as a diagnostic tool according to the Regulation (EU) 2017/745 of the European Parliament and of the Council of 5 April 2017 on medical devices [62]. It is important to keep in mind that for further development and fabrication of such devices, extensive quality controls must be followed during every step of the process. However, the product developed in this work is only applied for research (at the moment), and it is not subjected to these rules. Annex XV of this regulation lists the aspects that may directly affect research-only medical devices. Valid methodologies that are adapted to the device and the clinical outcome must be applied and addressed.

The skin equivalents developed in this work are included in the category of human skin models. According to the European Medicines Agency (EMA), these products are classified as tissue-engineered and cell therapy products, inside the category of Advanced Therapy Medicinal Products (ATMP). Such classification is dictated by the European Parliament Regulation (CE) Nº 1394/2007. Their application for translation into clinical use (clinical trials) must be regulated by the Good Manufacturing Procedures (GMP) guidelines, which are listed by the European Commission [63]. In this work the skin models were fabricated for research purposes only, so the GMPs did not need to be followed. However, the current laboratory biosafety regulations of Class II Biological Safety, listed in the Royal Decree 664/1997 and the European Parliament Directive 2000/54/CE, were followed during the whole research process.

The human skin equivalents grafted into mice were handled and developed under the proper regulations as well. Immunodeficient mice from the CIEMAT Laboratory Animals Facility (Spanish registration 28079-21) were housed in a pathogen-free environment following the European and Spanish regulations (Spanish R.D. 223/88 and O.M. 13-10-89 of the Ministry of Agricultural, Food and Fisheries, protection and use of animals in scientific research and internal biosafety and bioethics guidelines. European Convention 123 on use and protection of vertebrate mammals in experimentation and other scientific purposes). The skin models were made according to the procedure described under the patent WO2015173206 registered in 2015 by BioDan Group.

8.2. Socioeconomic Impact

This work introduces an important advance in the future diagnosis of EB. The principal characteristic of the developed device is its reduced size and manageability in comparison with other similar suction devices available for this purpose. This implies a significative cost reduction in materials, components, and general manufacturing, maintenance and repair. Hence, the applications in research and clinical fields could be considerably benefited in both the economic aspect and ease of use. Moreover, for future direct use on patients, it would imply a less invasive and painful diagnostic method, as there is no need for it to be attached to the skin for a long time. The applications in research are many, one of them explored in this work. To assess the results of gene editing approaches, having more parameters of the disease can verify the correction of the gene.

As it has been already mentioned, the impact in the field of Epidermolysis bullosa as a rare disease is important in several levels. Any progress made to make the lives of these patients easier is deeply significative. Additionally, the impact of such advances is related to the economy as well. Reducing diagnostic procedures lowers costs for both patients and the administration. The costs of the project are exposed in the following Tables 4 and 5. They have been divided on two parts: expenses of the device and of the skin models. As it can be seen, the total cost is around 970 €.

Table 4: *Expenses of suction device. Costs per unit and total cost displayed.*

Suction Device			
Material	Units	Cost per unit (€)	Total (€)
Blackhead Remover	1	20	20
Arduino-compatible Microcontroller	3	3.66	10.99
0.96” OLED Display	1	7.49	7.49
Incandescent Light Bulb	1	0.50	0.50
Pressure Sensor MPX4115A	1	17.82	17.82
Power Supply	1	10.99	10.99
Potentiometer	1	0.20	0.20
Pushbutton	1	0.30	0.30
Transistor BC547	1	0.20	0.20
Transistor TIP41	1	0.30	0.30
Resistor 220	3	0.05	0.15
Capacitor	1	0.20	0.20
Diode	1	0.50	0.50
Cable (10 m)	0.1	2.50	0.25
Solder	0.01	20	0.2

Total Cost (€)	70.09

Table 5: *Skin models expenses. Includes materials and reagents used in the experiments and laboratory equipment. Costs per unit and total cost displayed.*

Skin Models			
Experimental Materials			
Material	Units	Cost per unit (€)	Total (€)
DMEM 500 ml	5	27	135
Fetal Bovine Serum (FBS) 50 ml	0.5	32	16
Antibiotic/Antimicotic solution 100 ml	0.25	31.95	7.99
Trypsin 100 ml	1	15	15
Phosphate Buffered Saline (PBS) 500 ml	2	17	34
Tranexamic Acid 10 ml	0.01	314	3.14
Anti-Collagen VII 100 µl	0.05	289	14.45
Anti-Vimentin 100 µl	0.05	328	16.4
Anti-Keratin 10 100 µl	0.05	344	17.2
Anti-Keratin 14 100 µl	0.05	368	18.4
Secondary antibody 100 µl	0.1	340	34
ABC Kit	0.01	423.60	4.24
DAB Kit	0.01	152	1.52

Laboratory Equipment and Disposables			
Material	Units	Cost per unit (€)	Total (€)
Glass slides Thermo Scientific	2.5	80	200
2 ml stripette (200 pack)	2	67	134
5 ml stripette (200 pack)	2	67	134
10 ml stripette (200 pack)	0.5	67	33.5
15 ml tube (200 pack)	100	0.22	22
50 ml tube (200 pack)	50	0.24	12
1.5 ml Eppendorf tube (500 pack)	1	45	45
6-well plate (50 pack)	0.1	132	13.2
75 cm^2 culture flask (20 pack)	3	40	120
Filtration unit 250 ml (12 pack)	0.8	90.95	72.76
Nitrile gloves (100 pack)	2	9.68	19.36

Total Cost (€)	901

9. BIBLIOGRAPHY

[1] A. L. Mescher, *Junqueiras's Basic Histology Text and Atlas*, 13th ed. McGraw-Hill Education, 2013.

[2] B. Alberts, A. Johnson, J. Lewis, M. Raff, K. Roberts, and P. Walter, "Epidermis and its Renewal by Stem Cells," in *Molecular Biology of the Cell*, 4th ed., New York: Garland Science, 2002, p. Available from: https://www.ncbi.nlm.nih.gov/books.

[3] J. Kanitakis, "Anatomy, histology and immunohistochemistry of normal human skin," *Eur. J. Dermatology*, vol. 12, no. 4, pp. 390–9, 2001.

[4] R. Moll, M. Divo, and L. Langbein, "The human keratins: biology and pathology.," *Histochemistry and cell biology*, vol. 129, no. 6, pp. 705-33, Jun. 2008. Available: https://link.springer.com/article/10.1007%2Fs00418-008-0435-6

[5] J. Schweizer *et al.*, "New consensus nomenclature for mammalian keratins," *The Journal of Cell Biology*, vol. 174, no. 2, pp. 169-174, Jul. 2006. Available: https://www.ncbi.nlm.nih.gov/pmc/articles/PMC2064177/

[6] P. J. Koch and D. R. Roop, "The Role of Keratins in Epidermal Development and Homeostasis-Going Beyond the Obvious," *Journal of Investigative Dermatology*, vol. 123, no. 5, pp. x-xi, Nov. 2004. Available: https://www.jidonline.org/article/S0022-202X(15)32024-8/fulltext

[7] V. Haydont, B. A. Bernard, and N. O. Fortunel, "Age-related evolutions of the dermis: Clinical signs, fibroblast and extracellular matrix dynamics," *Mech. Ageing Dev.*, Mar. 2018.

[8] "The Function and Structure of the Skin | Plastic Surgery Key," 2016. [Online]. Available: https://plasticsurgerykey.com/the-function-and-structure-of-the-skin/. [Accessed: 03-Jun-2018].

[9] C. Has and J. Fischer, "Inherited epidermolysis bullosa: New diagnostics and new clinical phenotypes," *2018*, *Experimental Dermatology,* pp. 0-1. https://doi.org/10.1111/exd.13668

[10] L. R. A. Intong and D. F. Murrell, "Inherited epidermolysis bullosa: New diagnostic criteria and classification," *Clinics in Dermatology*, vol. 30, no. 1, pp. 70-77, 2012. Available: https://www.sciencedirect.com/science/article/pii/S0738081X11000885?via%3Dihub

[11] M. Laimer, G. Pohla-Gubo, A. Diem, C. Prodinger, J. W. Bauer, and H. Hintner, "Epidermolysis bullosa House Austria and Epidermolysis bullosa clinical network: Example of a centre of expertise implemented in a European reference network to face the burden of a rare disease," *Wiener Klinische Wochenschrift*, vol. 129, no. 1-2, pp. 1-7, 2017. Available: https://www.ncbi.nlm.nih.gov/pmc/articles/PMC5247537/

[12] J. Uitto, C. Has, H. Vahidnezhad, L. Youssefian, and L. Bruckner-Tuderman, "Molecular pathology of the basement membrane zone in heritable blistering diseases: The paradigm of epidermolysis bullosa," *Matrix Biollogy*, vol. 57-58, pp. 76-85, 2017. http://dx.doi.org/10.1016/j.matbio.2016.07.009

[13] J.-D. Fine, “Orphanet: Inherited epidermolysis bullosa,” *Orphanet Encyclopedia*, 2011. [Online]. Available: https://www.orpha.net/consor/cgi-bin/Disease_Search.php?lng=EN&data_id=11387&Disease_Disease_Search_diseaseGroup=epidermolysis-bullosa&Disease_Disease_Search_diseaseType=Pat&Disease(s)/group of diseases=Inherited-epidermolysis-bullosa&title=Inherited-. [Accessed: 25-May-2018].

[14] Commission of the European Communities, “Communication From The Commission to the European Parliament, the Council, the European Economic and Social Committee and The Committee of the Regions on Rare Diseases: Europe’s challenges.” 2008. Available: http://ec.europa.eu/health/ph_threats/non_com/docs/rare_com_en.pdf

[15] L. Bruckner-Tuderman and C. Has, “Molecular Heterogeneity of Blistering Disorders : The Paradigm of Epidermolysis Bullosa,” *The Journal of Investigative Dermatology*, vol. 132, pp. E2-E5, 2012. http://dx.doi.org/10.1038/skinbio.2012.2

[16] J.-D. Fine *et al.*, “The classification of inherited epidermolysis bullosa (EB): Report of the Third International Consensus Meeting on Diagnosis and Classification of EB,” *Journal of the American Academy of Dermatology,* vol. 58, no. 6, pp. 931-950, Jun. 2008. Available: https://www.jaad.org/article/S0190-9622(08)00208-9/fulltext

[17] M. Laimer, C. Prodinger, and J. W. Bauer, “Hereditary Epidermolysis bullosa,” *JDDG-Journal of the German Society of Dermatology*, vol. 13, no. 11, pp. 1125-1134, 2015. Available: https://onlinelibrary.wiley.com/doi/epdf/10.1111/ddg.12774

[18] L. Soro, C. Bartus, and S. Purcell, “Recessive Dystrophic Epidermolysis bullosa: A Review of Disease Pathogenesis and Update on Future Therapies.,” *The Journal of Clinical and Aesthetic Dermatology*, vol. 8, no. 5, pp. 41-6, May 2015. Avaliable: https://www.ncbi.nlm.nih.gov/pmc/articles/PMC4445895/

[19] M. Kim and D. F. Murrell, “Update on the pathogenesis of squamous cell carcinoma development in recessive dystrophic epidermolysis bullosa.,” *Eur. J. Dermatol.*, vol. 25 Suppl 1, pp. 30–32, Apr. 2015.

[20] L. R. A. Intong, “How to Take Skin Biopsies for Epidermolysis Bullosa,” *Dermatologic Clinics,* vol. 28, no. 2, pp. 197-200, Apr. 2010. Available: https://www.sciencedirect.com/science/article/pii/S0733863509001491?via%3Dihub

[21] E. Yiasemides, J. Walton, P. Marr, E. V Villanueva, and D. F. Murrell, “A comparative study between transmission electron microscopy and immunofluorescence mapping in the diagnosis of epidermolysis bullosa,” *The American Journal of Dermatopathology*, vol. 28, no. 5, pp. 387-394, 2006. DOI: 10.1097/01.dad.0000211510.44865.6d

[22] B. R. Webber *et al.*, “CRISPR/Cas9-based genetic correction for recessive dystrophic epidermolysis bullosa,” *NPJ Regen. Med.*, vol. 1, p. 16014, Dec. 2016. Available: https://www.ncbi.nlm.nih.gov/pubmed/28250968

[23] M. F. Jonkman and A. M. G. Pasmooij, “Realm of Revertant Mosaicism Expanding,” *Journal of Investigative Dermatology*, vol. 132, no. 3, pp. 514-516, Mar. 2012. Available: https://www.sciencedirect.com/science/article/pii/S0022202X1535630X?via%3Dihub

[24] T. Wong *et al.*, “Potential of Fibroblast Cell Therapy for Recessive Dystrophic Epidermolysis Bullosa,” *Journal of Investigative Dermatology*, vol. 128, no. 9, pp. 2179-2189, Sep. 2008. Available: https://www.jidonline.org/article/S0022-202X(15)34026-4/fulltext

[25] E. Rashidghamat, J. E. Mellerio, A. E. Martinez, and J. A. McGrath, “Mesenchymal stem cell therapy for recessive dystrophic epidermolysis bullosa: prospects and clinical progress,” *Expert Opinion on Orphan Drugs*, vol. 4, no. 4, pp. 343-345, 2016. Available: https://www.tandfonline.com/doi/full/10.1517/21678707.2016.1152886

[26] D. Wenzel, J. Bayerl, A. Nystrom, L. Bruckner-Tuderman, A. Meixner, and J. M. Penninger, “Genetically corrected iPSCs as cell therapy for recessive dystrophic epidermolysis bullosa.,” *Sci. Transl. Med.*, vol. 6, no. 264, p. 264ra165, Nov. 2014.

[27] M. Carretero, S. Guerrero-Aspizua, and M. del Río, “Applicability of bioengineered human skin: from preclinical skin humanized mouse models to clinical regenerative therapies,” *Bioengineered Bugs*, vol. 2, no. 4, pp. 203-207, 2011. Available: https://e-archivo.uc3m.es/bitstream/handle/10016/20256/applicability_BB_2011_ps.pdf?sequence=1&isAllowed=y

[28] A. Meana *et al.*, “Large surface of cultured human epithelium obtained on a dermal matrix based on live fibroblast-containing fibrin gels,” *Burns*, vol. 24, no. 7, pp. 621-630, Nov. 1998. Available: https://www.burnsjournal.com/article/S0305-4179(98)00107-7/fulltext

[29] S. Negri, G. Federici, S. Farinato, and C. Fila, “Human plasma as a dermal scaffold for the generation of a completely autologous bioengineered skin,” *Journal of Clinical Rehabilitative Tissue Engineering Research*, vol. 13, no. 47, pp. 9211-9216, 2009. Available: https://www.researchgate.net/publication/286497840_Human_plasma_as_a_dermal_scaffold_for_the_generation_of_a_completely_autologous_bioengineered_skin [30] Arduino, “What is Arduino.” [Online]. Available: https://www.arduino.cc/en/Guide/Introduction. [Accessed: 23-Apr-2018].

[30] Arduino, “What is Arduino.” [Online]. Available: https://www.arduino.cc/en/Guide/Introduction. [Accessed: 23-Apr-2018].

[31] Atmel, “ATmega328/P,” *AVR Microcontrollers*, p. 442, 2016. Available: http://ww1.microchip.com/downloads/en/DeviceDoc/Atmel-42735-8-bit-AVR-Microcontroller-ATmega328-328P_Datasheet.pdf

[32] Vac Acero International, “Oil Sealed Rotary Vane Pumps, Part 1,” 2016. [Online]. Available: https://vacaero.com/information-resources/vacuum-pump-technology-education-and-training/1040-oil-sealed-rotary-vane-pumps-part-1.html. [Accessed: 07-Jun-2018].

[33] L. Shenzhen longyi Technology Co., “Vacuum pump LY370CPM.” [Online]. Available: http://www.longykj.com/en/productshow.asp?ArticleID=249. [Accessed: 09-May-2018].

[34] Freescale, “Freescale Semiconductor Integrated Silicon Pressure Sensor On-Chip Signal Conditioned, Temperature Compensated and Calibrated,” *Sensors (Peterborough, NH)*, pp. 2007-2009, 2009. Available: https://cdn.sos.sk/productdata/3f/c3/6bfaacf8/mpx-5999-d.pdf

[35] R. S. Kraleva and V. Kralev, “Mathematics and Natural Philosophy - Estimation of the error of the silicon based pressure sensor MPX4115A at room ambient

temperatures," *Niels Bohr Collect. Work.*, vol. 11, no. C, pp. 667–673, 2005.

[36] C. Platt, *Encyclopedia of Electronic Components Volume 2*. Maker Media, 2015.

[37] C. Platt, *Encyclopedia of Electronic Components Volume 1 Resistors, Capacitors, Inductors, Switches, Encoders, Relays, Transistors*. 2013.

[38] S. Systech, "SSD1306 Advance Information," *Rivers*, pp. 1–50, 2005.

[39] AZ Delivery, "0.96 inch I2C OLED display AZ Delivery." [Online]. Available: https://www.az-delivery.de/products/0-96zolldisplay#description. [Accessed: 19-May-2018].

[40] J. A. Langbridge, *Arduino Sketches: Tools and Techniques for Programming Wizardry*. Wiley, 2015.

[41] T. L. Floyd, *Electronic Devices*, *Electron Flow Version.* 9th ed., Pearson Education, 2008.

[42] A. Robbins and W. Miller, *Circuit analysis: theory and practice*. 5th ed. Cengage Learning, 2013.

[43] P. Unna, "Zur Anatomie der Blasenbildung an der menschlichen Haut," *Vjschr. Derm. Syph*, vol. 5, no. 1, 1878.

[44] I. H. Blank and O. G. Miller, "A method for the separation of the epidermis from the dermis.," *The Journal of Investigative Dermatology.*, vol. 15, no. 1, pp. 9-10, 1950.

[45] U. Kiistala and K. K. Mustakallio, "In-vivo separation of epidermis by production of suction blisters," The *Lancet*, vol. 283, no. 7348, pp. 1444-1445, 1964.

[46] U. Kiistala and K. K. Mustakallio, "Dermo-Epidermal Separation with Suction: Electron Microscopic and Histochemical Study of Initial Events of Blistering on Human Skin," *The Journal of Investigative Dermatology*, vol. 48, no. 5, pp. 466-477, May 1967. Available: https://ac.els-cdn.com/S0022202X15473117/1-s2.0-S0022202X15473117-main.pdf?_tid=c569e7c8-4cc4-4828-a951-33500ca25a0e&acdnat=1528922074_18ccfa5b8b2ddba5d94425a76c0c56bc

[47] W. Ray Gammon, R. A. Briggaman, A. O. Inman, L. L. Queen, and C. E. Wheeler, "Differentiating Anti-Lamina Lucida and Anti-Sublamina Densa Anti-BMZ Antibodies by Indirect Immunofluorescence on 1.0 M Sodium Chloride-Separated Skin," *The Journal of Investigative Dermatology.*, vol. 82, no. 2, pp. 139-144, Feb. 1984. Available: https://www.sciencedirect.com/science/article/pii/S0022202X15433081

[48] L. K. Hatje, C. Richter, U. Blume-Peytavi, and J. Kottner, "Blistering time as a parameter for the strength of dermoepidermal adhesion: A systematic review and meta-analysis," *British Journal of Dermatology*, vol. 172, no. 2, pp. 323-330, 2015. Available: https://onlinelibrary.wiley.com/doi/full/10.1111/bjd.13298

[49] M. J. Tidman and R. A. Eady, "Evidence for a functional defect of the lamina lucida in recessive dystrophic epidermolysis bullosa demonstrated by suction blisters.," *Br. J. Dermatol.*, vol. 111, no. 4, pp. 379–87, Oct. 1984.

[50] C. Feliciani *et al.*, "'Suction split' as a routine method to differentiate epidermolysis bullosa acquisita from bullous pemphigoid," *Journal of the European Academy of Dermatology and Venereology*, vol. 10, no. 3, pp. 243-247, 1998. Available: https://europepmc.org/abstract/med/9643329

[51] G. Petrof *et al.*, "Potential of Systemic Allogeneic Mesenchymal Stromal Cell

Therapy for Children with Recessive Dystrophic Epidermolysis Bullosa," *Journal of Investigative Dermatology*, vol. 135, no. 9, pp. 2319-2321, Sep. 2015. Available: https://www.jidonline.org/article/S0022-202X(15)39008-4/fulltext

[52] J. Nazaroff, S. Li, A. Lane, M. Marinkovich, and J. Tang, "601 Measurement of skin adherence in recessive dystrophic epidermolysis bullosa patients," *J. Invest. Dermatol.*, vol. 138, no. 5, p. S102, May 2018.

[53] J. Sun, *Dynamics and Control of Switched Electronic Systems*, 1st ed. Springer-Verlag London, 2012.

[54] A. Hovnanian *et al.*, "Characterization of 18 new mutations in COL7A1 in recessive dystrophic epidermolysis bullosa provides evidence for distinct molecular mechanisms underlying defective anchoring fibril formation.," *Am. J. Hum. Genet.*, vol. 61, no. 3, pp. 599–610, Sep. 1997.

[55] M. J. Escámez *et al.*, "The first COL7A1 mutation survey in a large Spanish dystrophic epidermolysis bullosa cohort: C.6527insC disclosed as an unusually recurrent mutation," *Br. J. Dermatol.*, vol. 163, no. 1, pp. 155–161, 2010.

[56] ATCC, "Formulation for Dulbecco's Modified Eagle's Medium (DMEM) ATCC® 30-2002". Available: https://www.atcc.org/~/media/D7399222FD8B4EF68FD56DD8058804BA.ashx

[57] J. G. Rheinwald and H. Green, "Serial cultivation of strains of human epidermal keratinocytes: the formation of keratinizing colonies from single cells," *Cell*, vol. 6, no. 3, pp. 331-43, Nov. 1975. Available: https://www.ncbi.nlm.nih.gov/pubmed/1052771 [56] S. Yang *et al.*, "Generation of Retroviral Vector for Clinical Studies Using Transient Transfection," *Hum. Gene Ther.*, vol. 10, no. 1, pp. 123–132, Jan. 1999.

[58] S. Yang *et al.*, "Generation of Retroviral Vector for Clinical Studies Using Transient Transfection," *Human Gene Therapy*, vol. 10, no. 1, pp. 123-132, Jan. 1999. Available: https://www.ncbi.nlm.nih.gov/pubmed/10022537

[59] V. Vengelen-Tyler and American Association of Blood Banks, *Technical manual*, 13th ed. Bethesda MD: American Association of Blood Banks, 1999.

[60] D. Cadena-Herrera *et al.*, "Validation of three viable-cell counting methods: Manual, semi-automated, and automated," *Biotechnology Reports*, vol. 7, pp. 9-16, Sep. 2015. Available: https://www.sciencedirect.com/science/article/pii/S2215017X15000235

[61] L. Martínez Santamaría, "Desarrollo de modelos preclínicos de regeneración cutánea deteriorada," Tesis doctoral. Dep. Bioquímica y Biología Molecular. Universidad Complutense, Madrid, 2010.

[62] European Parliament and Council of the European Union, "Regulation (EU) 2017/745 of the European Parliament and of the Council of 5 April 2017 on medical devices," *Off. J. Eur. Union*, vol. 60, no. April 2014, pp. 1–175, 2017.

[63] European Medicines Agency, "Good Manufacturing Practice for Advanced Therapy Medicinal Products," vol. 4, no. November 2017, 2017.

ANNEX

Epidermolysis bullosa types and subtypes. Includes inheritance patterns (AR: autosomal recessive; AD: autosomal dominant), mutated genes and affected proteins of each. [17]

EB (sub-) type	Inheritance	Mutated gene	Affected protein
Epidermolysis bullosa simplex, EBS (intradermal [epidermolytic] blisters)			
Suprabasal EBS (cytolysis of suprabasal keratinocytes)			
Acral peeling skin syndrome	AR	*TGM5*	Transglutaminase-5
Superficial EBS	AD	?	?
Acantholytic EBS (includesvariants formerly termed lethal acantholytic EBS and lethal congenital EBS)	AR	DSP, JUP	Desmoplakin, plakoglobin
Skin fragility syndromes (very rare variants)			
Desmoplakin deficiency (skin fragility/woolly hair syndrome)	AR	DSP	Desmoplakin
Plakoglobin deficiency	AR	JUP	Plakoglobin
Plakophilin deficiency (skin fragility/ectodermal dysplasia syndrome)	AR	PKP1	Plakophilin1
Basal EBS (cytolysis of basal keratinocytes)			
Localized EBS (formerly type Webwer-Cockayne)	AD	KRT5, KRT14	Keratin 5, keratin 14
Generalized severe EBS (formerly type Dowling-Meara, herpetiform EBS)	AD	KRT5, KRT14	Keratin 5, keratin 14
Generalized intermediate EBS (formerly EBS, generalized-other; non-Dowling-Meara; EBS, type Koebner)	AD	KRT5, KRT14, COL17A1	Keratin 5, keratin 14, type XVII collagen
EBS with mottled pigmentation	AD	KRT5	Keratin 5
EBS with migratory circinate erythema	AD	KRT5	Keratin 5
Autosomal-recesive EBS K14	AR	KRT14	Keratin 14
Trauma-induced skin blistering	AR	EXPH5	Exophilin-5
EBS with muscle dystrophy	AR	PLEC1	Plectin
EBS with pyloric atresia	AR	PLEC1, ITGA6, ITGB4	Plectin, integrin α6, integrin β4
EBS type Ogna	AD	PLEC1	Plectin
Autosomal-recessive EBS, BP230 deficiency	AR	DST	Bullous pemphigoid antigen 1 (BP230)
Autosomal-recessive EBS, exophilin-5 deficiency	AR	EXPH5	Exophilin 5
Junctional epidermolysis bullosa, JEB (junctional [lucidolytic] blisters within the basement membrane zone)			
Generalized JEB			
Generalized severe JEB (previously type Herlitz)	AR	LAMA3, LAMB3, LAMC2	Laminin α3, β3, γ2 laminin 332 chain

Generalized intermediate JEB (formerly type non-Herlitz; JEB, generalized other; GABEB)	AR	LAMA3, LAMB3, LAMC2	Laminin α3, β3, γ2 laminin 332 chain
JEB with pyloric atresia	AR	ITGA6, ITGB4	Integrin α6, integrin β4
JEB, late onset (formerly progressive)	AR	COL17A1	Type XVII collagen
Localized JEB	AR	COL17A1	Type XVII collagen
JEB with respiratory and renal involvement (previously EB congenital nephrotic syndrome-interstitial lung disease)	AR	ITGA3	Integrin A3
Localized JEB			
Localized JEB (previously localized JEB, non-Herlitz)	AD	COL17A1	Type XVII collagen
JEB inversa	AR	LAMA3, LAMB3, LAMC2	Laminin α3, β3, γ2-chains of laminin 332
JEB, laryngo-onycho-cutaneous syndromes	AR	LAMA3A	Laminin α3a chain of laminin332
Dystrophic epidermolysis bullosa, DEB (dermolytic blistering below the lamina densa)			
Dominant DEB			
Generalized dominant DEB (formerly type Pasini, Cockayne-Touraine)	AD	COL7A1	Type VII collagen
Acral dominant DEB	AD, AR	COL7A1	Type VII collagen
Pretibial dominant DEB	AD, AR	COL7A1	Type VII collagen
Dominant DEB pruriginosa	AD, AR	COL7A1	Type VII collagen
Dominant DEB, nails only	AD	COL7A1	Type VII collagen
Dominant DEB, bullous dermolysis of the new born	AD, AR	COL7A1	Type VII collagen
Recessive DEB			
Generalized severe DEB (formerly type Hallopeau-Siemens)	AR	COL7A1	Type VII collagen
Generalized intermediate DEB (formerly type non-Hallopeau-Siemens; RDEB, generalized other)	AR	COL7A1	Type VII collagen
Recessive DEB inversa	AR	COL7A1	Type VII collagen
Localized recessive DEB (formerly acral recessive DEB)	AR	COL7A1	Type VII collagen
Pretibial recessive DEB	AD, AR	COL7A1	Type VII collagen
Recessive DEB pruriginosa	AR	COL7A1	Type VII collagen
Recessive DEB (centripetal variant)	AR	COL7A1	Type VII collagen
Recessive DEB, bullous dermolysis of the newborn	AR	COL7A1	Type VII collagen
Kindler syndrome (intraepidermal, junctional or sub-lamina-densa blisters	AR	FERMT1 (KIND1)	Fermitin family homo-log 1 protein (kindlin-1)